CHALMERS

Multiscale Techniques in Linear Elasticity

Master's Thesis in Engineering Mathematics

ROBERT FORSLUND

Department of Mathematical Sciences
Chalmers University of Technology
Göteborg, Sweden 2015

Master's Thesis in Engineering Mathematics

Multiscale Techniques in Linear Elasticity

Robert Forslund

Department of Mathematical Sciences
Chalmers University of Technology
Göteborg, Sweden 2015

Multiscale Techniques in Linear Elasticity
ROBERT FORSLUND

Department of Mathematical Sciences
Chalmers University of Technology
SE-412 96 Göteborg
Sweden
Telephone +46 (0)31-772 1000

Matematiska vetenskaper
Göteborg, Sweden 2015

Abstract

We use a local orthogonal decomposition (LOD) technique to derive a finite element method for planar linear elasticity problems with strongly heterogeneous material data and inhomogeneous Dirichlet and Neumann boundary conditions. These problems are becoming more and more relevant due to the increasing use of composite materials. We apply our generalized finite element method in numerical experiments and observe optimal convergence rates in the energy norm. We also prove an a posteriori error estimate for the method and use it to propose a basic adaptive algorithm for error reduction.

Keywords: finite element method, multiscale method, LOD, mixed boundary conditions, a posteriori error estimate, linear elasticity, composite material.

Acknowledgements

First of all I would like to thank my supervisor Axel Målqvist for his invaluable guidance and constant support throughout this thesis work. I would also like to thank Anna Persson for sharing her insights during the implementation process. They helped a great deal. Finally, I would like to thank Fredrik Larsson for providing information on homogenization techniques.

Robert Forslund
Göteborg, June 2015

Contents

1

Introduction

In multiscale problems the data varies over multiple scales in space or time. Some problems with this multiscale structure are mathematically described by partial differential equations. Examples include structural mechanics applications with composite materials.

A composite material is a combination of different materials and can be designed to have specific properties. It consists of a binding material, also referred to as the matrix, and reinforcement. The reinforcement is made out of different fibers or fragments that are surrounded and held in place by the matrix. The combined materials are partitioned in the sense that there is a recognizable interface between them. This structure can give a composite material certain properties that are preferable over the ones of its constituents. Several applications benefit from composite materials. Carbon fiber reinforced materials are extremely strong for their weights and are for example used in vehicle bodies to reduce fuel consumption. Ceramic matrix composites can withstand high temperatures, which makes them useful for improving engine efficiency. These are only a few examples.

Composite materials are heterogeneous and may have structures that vary over multiple scales. These variations become problematic when computer simulations are performed as an aid in designing materials. In such simulations, partial differential equations are solved numerically, often using finite elements. In the standard finite element method (FEM), the variations in the fine scales need to be resolved by one global mesh, which is costly. Several multiscale methods (see Section 1.2 in [7] for a review) have been developed and are used to avoid this problem. Some of them capture the fine scale structure of the solution via localized basis functions. This work focuses on a particular multiscale method that employs this technique. It is called local orthogonal decomposition (LOD) method and was first proposed in [14] for elliptic problems with a heterogeneous diffusion matrix and homogeneous Dirichlet boundary. In [8] the method was developed further by allowing inhomogeneous and mixed boundary conditions and using an improved localization strategy. Furthermore, an a priori estimate that shows convergence of the method was provided.

The LOD method is derived from the variational multiscale method [10] framework in the sense that it in its first step splits a finite element space into a coarse space and a fine space. The LOD method has advantages over other methods because it does not rely on certain assumptions on the data, like complete scale separation or periodicity. In this work the method is applied to elasticity problems.

1.1 Purpose and scope of thesis

The LOD method is relatively recent and it is therefore of interest to use it in different problems where it is expected to display good results. With this background in mind, we formulate the purpose of this thesis as follows. The purpose is to use the LOD method to solve linear elasticity problems involving heterogeneous materials, and to prove an a posteriori error estimate that can be utilized by an adaptive algorithm that reduces the error between the LOD approximation and the exact solution.

We restrict ourselves to the planar problem. It is important to note that the three-dimensional problem is treated similarly. While the finite element methods in this thesis are formulated for the planar problem, they could easily be reformulated for the three-dimensional problem by adjusting the exposition in an obvious way. The sole reason for making this restriction is that it allows for a simpler implementation that is more suitable for this thesis work.

The structure of the thesis is as follows. In Chapter 2 we study the elasticity problem and lay the foundation of the subsequent chapters. We introduce the LOD method in Chapter 3, give an overview of the implementation of an LOD solver in Chapter 4, prove an a posteriori error estimate and describe an adaptive algorithm in Chapter 5, and present some experiments in Chapter 6.

1.2 Notation

We need to define some operators. Let p, $v = (v_1, v_2)^{\mathrm{t}}$ and $\tau = \left(\begin{smallmatrix} \tau_{11} & \tau_{12} \\ \tau_{21} & \tau_{22} \end{smallmatrix}\right)$ be real-valued functions of two (spatial) variables $(x, y)^{\mathrm{t}}$. Let

$$
\begin{aligned}
\nabla p &= \begin{pmatrix} \partial p/\partial x \\ \partial p/\partial y \end{pmatrix}, \\
\nabla \cdot v &= \partial v_1/\partial x + \partial v_2/\partial y, \\
\nabla v &= \begin{pmatrix} \partial v_1/\partial x & \partial v_1/\partial y \\ \partial v_2/\partial x & \partial v_2/\partial y \end{pmatrix}, \\
\nabla \cdot \tau &= \begin{pmatrix} \partial \tau_{11}/\partial x + \partial \tau_{12}/\partial y \\ \partial \tau_{21}/\partial x + \partial \tau_{22}/\partial y \end{pmatrix}.
\end{aligned}
$$

Furthermore, define the inner product : of two 2×2 matrices by

$$\sigma : \tau = \sum_{i,j=1}^{2} \sigma_{ij}\tau_{ij}.$$

Let $L^2(\Omega)$ denote the space of square-integrable scalar-valued functions on a domain $\Omega \supseteq K$ equipped with the inner product and norm

$$(p, q)_{L^2(K)} = (p, q)_K = \int_K p\, q \,\mathrm{d}x\,, \quad \|p\|_{L^2(K)} = \|p\|_K = \sqrt{(p, p)_K}$$

and, analogously, let $\underset{\sim}{L}^2$ and $\underset{\approx}{L}^2$ be the corresponding spaces of vector-valued and matrix-valued functions, respectively, with inner products and norms

$$(u, v)_{\underset{\sim}{L}^2(K)} = (u, v)_K = \int_K u \cdot v \,\mathrm{d}x\,, \quad \|u\|_{\underset{\sim}{L}^2(K)} = \|u\|_K = \sqrt{(u, u)_K},$$

$$(\sigma, \tau)_{\underset{\approx}{L}^2(K)} = (\sigma, \tau)_K = \int_K \sigma : \tau \,\mathrm{d}x\,, \quad \|\sigma\|_{\underset{\approx}{L}^2(K)} = \|\sigma\|_K = \sqrt{(\sigma, \sigma)_K}.$$

For these three spaces, we will use the convention of excluding the subscript in their corresponding inner products if they are taken over the entire domain Ω, i.e. if $K = \Omega$.

Other spaces of vector valued functions can also be defined by extending the corresponding space for scalar valued functions. For example, denote by $\underset{\sim}{H}^k$ the Sobolev space of all v whose weak partial derivatives of order less than or equal to k belong to $\underset{\sim}{L}^2$. Its inner product, norm and seminorm are the natural extensions of those of H^k. Most importantly, $\underset{\sim}{H}^1$ has the inner product $(u, v)_{\underset{\sim}{H}^1(K)} = (u, v)_K + (\nabla u, \nabla v)_K$, with the corresponding norm defined by $\|u\|^2_{\underset{\sim}{H}^1(K)} = \|u\|^2_K + \|\nabla u\|^2_K$.

2

The planar linear elasticity problem

In this chapter we present the model problem and its weak formulation. We also formulate the standard FEM and show a standard error estimate.

Let $\Omega \subset \mathbb{R}^2$ be a polygonal domain with boundary $\partial\Omega = \Gamma_D \cup \Gamma_N$, where Γ_D and Γ_N are disjoint and $\text{meas}(\Gamma_D) > 0$. Let $u = (u_1, u_2)^{\text{t}}$ be a displacement, where u_1 and u_2 denote a horizontal and vertical displacement, respectively. An (infinitesimal) rectangular element $\omega \subseteq \Omega$ can be affected by a whole body load and its boundary $\partial\omega$ can be affected by traction. Let $f = (f_1, f_2)^{\text{t}}$ denote a whole body load in force per unit area. Let $\sigma = \left(\begin{smallmatrix} \sigma_{11} & \sigma_{12} \\ \sigma_{21} & \sigma_{22} \end{smallmatrix}\right)$ be the stress matrix. For instance, σ_{12} expresses the force per unit length in the x-direction on an edge with unit normal in the y-direction. The stress matrix σ is symmetric due to the conservation of angular momentum. In linear elasticity we assume that displacements, displacement gradients, and rotations of a body are small, meaning that the strain, which measures deformation, is small. The strain matrix is then given by

$$\varepsilon(u) = \frac{1}{2}\left(\nabla u + (\nabla u)^{\text{t}}\right). \tag{2.1}$$

Note that ε is symmetric as well. Furthermore, we assume that the needed constitutive relationship between the stress and strain is linear. This relationship is called Hooke's law, which in its general form contains a fourth-order stiffness tensor that describes the material. If the material is isotropic, i.e. has the same properties in all directions, Hooke's law can be written as

$$\sigma(u) = 2\mu\varepsilon(u) + \lambda\,(\nabla \cdot u)\,I, \tag{2.2}$$

where μ and λ are positive and material specific parameters known as the Lamé parameters. The parameter μ is the shear modulus and $\lambda = J - 2\mu/3$, where J is the bulk modulus. Both parameters have the unit N/m^2 (but we reduce it to N/m in the planar

case). Observe that heterogeneous materials are generally not isotropic. However, the isotropic model (2.2) can be used for anisotropic materials as well as long as the domain is well resolved. In this case, the material can be assumed to be locally isotropic even if it displays anisotropy on the larger scales, and consequently we can use Lamé parameters that are bounded but may vary in space.

Three-dimensional problems can often be reduced to two-dimensional ones by using two types of configurations called plane strain and plane stress. Plane strain can be assumed for long, slender structures, where the strains associated with the length direction are negligible. Therefore, it suffices to only study a cross-section. Plane stress can be assumed for thin plates when there is no stress acting on the two main surfaces. In this thesis we solve problems of plane strain only. However, problems of plane stress are solved analogously because the only difference between the two cases is the choice of elasticity matrix (to be introduced in Chapter 4).

Locking is a phenomenon that occurs when λ approaches ∞, meaning that the elastic material becomes nearly incompressible. This special case produces difficulties that require strategies that are beyond the topic in this report. Therefore, we do not consider problems where locking is an issue.

The problem of interest is a system of linear partial differential equations (in u and σ) with a mixed boundary condition, given by

$$
\begin{aligned}
(Cauchy's\ equilibrium\ eq.) \qquad -\nabla \cdot \sigma(u) &= f && \text{in } \Omega, && (2.3a)\\
(Hooke's\ law) \qquad \sigma(u) &= 2\mu\varepsilon(u) + \lambda\,(\nabla \cdot u)\, I && \text{in } \Omega, && (2.3b)\\
(Displacement) \qquad u &= g_D && \text{on } \Gamma_D, && (2.3c)\\
(Traction) \qquad \sigma(u)\, n &= g_N && \text{on } \Gamma_N. && (2.3d)
\end{aligned}
$$

I is the 2–by–2 identity matrix and n is the unit outer normal of $\partial\Omega$. We shall seek the vector valued displacement function $u = (u_1, u_2)^{\mathrm{t}}$.

2.1 Weak formulation of the problem

For the remainder of this thesis we use the notation $a \lesssim b$ to mean $a \leq Cb$ where C is a positive constant that may depend on Ω, the bounds of μ and λ, and the shape regularity of the triangulations introduced later on. At the same time, C does not depend on the mesh sizes of these triangulations, nor on the variations in μ, λ, f, g_D, and g_N. We use the symbol $\gtrsim$ analogously.

We derive the weak formulation of (2.3). Let

$$
\underset{\sim}{V} = \left\{ v \in \underset{\sim}{H}^1(\Omega) : v|_{\Gamma_D} = (0,0)^{\mathrm{t}} \right\}.
$$

Multiply (2.3a) with a test function $v \in \underset{\sim}{V}$ and integrate by parts to get

$$
\int_\Omega f \cdot v \,\mathrm{d}x = \int_\Omega \sigma(u) : \nabla v \,\mathrm{d}x - \int_{\Gamma_N} \underbrace{\sigma(u)\, n}_{g_N} \cdot v \,\mathrm{d}s. \tag{2.4}
$$

Decompose ∇v into its symmetric part $\frac{1}{2}\nabla v + \frac{1}{2}(\nabla v)^{\mathrm{t}}$ and antisymmetric part $\frac{1}{2}\nabla v - \frac{1}{2}(\nabla v)^{\mathrm{t}}$.[1] Then, since $\sigma(u)$ is symmetric, we have

$$\sigma(u) : \nabla v = \sigma(u) : \varepsilon(v) + \sigma(u) : \frac{1}{2}\left(\nabla v - (\nabla v)^{\mathrm{t}}\right) = \sigma(u) : \varepsilon(v). \tag{2.5}$$

Insert (2.5) and (2.3b) into (2.4) to get

$$\begin{aligned}\int_\Omega f \cdot v \,\mathrm{d}x + \int_{\Gamma_N} g_N \cdot v \,\mathrm{d}s &= \int_\Omega \left(2\mu\varepsilon(u) + \lambda(\nabla \cdot u)I\right) : \varepsilon(v) \,\mathrm{d}x \\ &= \int_\Omega \left(2\mu\varepsilon(u) : \varepsilon(v) + \lambda \nabla \cdot u \, \nabla \cdot v\right) \,\mathrm{d}x,\end{aligned}$$

where we have used that $I : \varepsilon(v) = \nabla \cdot v$. Hence the weak formulation of (2.3) is the following:

$$\text{find } u \in \underset{\sim}{H}^1(\Omega) \text{ such that } u|_{\Gamma_D} = g_D \text{ and } a(u,v) = L(v) \quad \forall v \in \underset{\sim}{V}, \tag{2.6}$$

where

$$\begin{aligned}a(u,v) &= \int_\Omega \left(2\mu\varepsilon(u) : \varepsilon(v) + \lambda \nabla \cdot u \, \nabla \cdot v\right) \,\mathrm{d}x, \\ L(v) &= \int_\Omega f \cdot v \,\mathrm{d}x + \int_{\Gamma_N} g_N \cdot v \,\mathrm{d}s.\end{aligned}$$

As a bilinear form in the Hilbert space $\left(\underset{\sim}{V}, (\,\cdot\,,\cdot\,)_{\underset{\sim}{H}^1(\Omega)}\right)$, $a(\,\cdot\,,\cdot\,)$ is bounded since

$$|a(u,v)| \overset{(2.1)}{\lesssim} \|\nabla u\|\|\nabla v\| + \|\nabla \cdot u\|\|\nabla \cdot v\| \lesssim \|\nabla u\|\|\nabla v\| \lesssim \|u\|_{\underset{\sim}{H}^1(\Omega)}\|v\|_{\underset{\sim}{H}^1(\Omega)} \tag{2.7}$$

for all $u, v \in \underset{\sim}{V}$, where we use that $\|\nabla \cdot u\| \leq 2\|\nabla u\|$. In order to show that $a(\,\cdot\,,\cdot\,)$ is coercive on $\underset{\sim}{V}$ we make use of the following theorem.

THEOREM 2.1 (special case of Korn's inequality). *Let* $\mathrm{meas}(\Gamma_{\mathrm{D}}) > 0$. *Then*

$$\|\varepsilon(v)\| \gtrsim \|v\|_{\underset{\sim}{H}^1(\Omega)} \quad \forall v \in \underset{\sim}{V}.$$

A proof of this theorem can be found in [2]. Theorem 2.1 gives

$$a(v,v) \gtrsim \|\varepsilon(v)\|^2 + \|\nabla \cdot v\|^2 \gtrsim \|\varepsilon(v)\|^2 \gtrsim \|v\|^2_{\underset{\sim}{H}^1(\Omega)} \quad \forall v \in \underset{\sim}{V}. \tag{2.8}$$

The bilinear form $a(\,\cdot\,,\cdot\,)$ is symmetric and positive-definite, and thus defines an inner product on $\underset{\sim}{V}$. We define the energy norm $|||\cdot||| = \sqrt{a(\,\cdot\,,\cdot\,)}$ and apply the same notation as for the $\underset{\sim}{L}^2$ inner product and norm, i.e. we use a subscript as in $a(\,\cdot\,,\cdot\,)_K$ and $|||\cdot|||_K$ only if the product is taken over a strict subset K of Ω. The energy norm is equivalent to both $\|\cdot\|_{\underset{\sim}{H}^1(\Omega)}$ and $\|\nabla \cdot\|$ due to (2.7) and (2.8).

[1] Physically, this means that the displacement gradient ∇v is expressed as the sum of an infinitesimal strain matrix and an infinitesimal rotation matrix.

Now, in order to show that (2.6) has a unique solution, assume that $g_D = u_0|_{\Gamma_D}$ for some $u_0 \in \underset{\sim}{H}^1(\Omega)$. Then we can write $u = u_0 + w$ for some $w \in \underset{\sim}{V}$, meaning that (2.6) is equivalent to the following formulation, in which the trial space and test space are the same.

$$\text{Find } w \in \underset{\sim}{V} \text{ such that } a(w, v) = L(v) - a(u_0, v) = F(v) \quad \forall v \in \underset{\sim}{V}. \tag{2.9}$$

But it follows from (2.7), (2.8), the fact that $F(v)$ is a bounded linear functional on $\underset{\sim}{V}$, and, consequently, Lax-Milgram theorem that this problem has a unique solution, which implies that (2.6) also has a unique solution $u = u_0 + w$ that is independent of the choice of the extension u_0. The above results amount to the following theorem.

THEOREM 2.2 (solution of weak formulation). *Assume that* $f \in \underset{\sim}{L}^2(\Omega)$, $g_D = u_0|_{\Gamma_D}$ *where* $u_0 \in \underset{\sim}{H}^1(\Omega)$, $g_N \in \underset{\sim}{L}^2(\Gamma_N)$, *and* $\text{meas}(\Gamma_D) > 0$. *Then the variational formulation* (2.6) *has the unique solution* $u \in \underset{\sim}{H}^1(\Omega)$.

Note that the assumption $\text{meas}(\Gamma_D) > 0$ is made throughout this chapter. This assumption excludes the pure traction problem, in which $\Gamma_N = \partial\Omega$. In the pure traction problem the body is not necessarily constrained in terms of displacement. This means that a compatibility condition, namely that the system of forces (body forces and tractions) is equivalent to zero under infinitesimal rigid motion (see Section 3.4 in [6]), needs to be satisfied in order for (2.6) to be solvable. The solution has the property that its mean displacement and rotation in Ω are zero. We pay no further attention to the pure traction problem here.

2.2 Standard finite element method

Let $\mathcal{T}_h$ be a geometrically conforming, shape regular triangulation of Ω and let

$$\underset{\sim}{V}_h = \{v \in \underset{\sim}{V} : v|_T \text{ is affine } \forall T \in \mathcal{T}_h\}$$

be a space of piecewise affine functions in $\underset{\sim}{V}$. Let $h_T = \text{diam}(T)$ and let $h = \max_{T\in\mathcal{T}_h} h_T$ denote the mesh size of $\mathcal{T}_h$. We assume that h is sufficiently small so that $\mathcal{T}_h$ resolves all the possible variations in the data. Let $\{N_i\}_{i=1}^n = \mathcal{N}_h$ be the set of Lagrange points of $\mathcal{T}_h$, i.e. the set of node points located at the triangle vertices.

In order to formulate the Galerkin approximation problem corresponding to (2.5), let $u_{0,h}$ be a continuous piecewise affine function on $\mathcal{T}_h$ such that

$$u_{0,h}(z) = \begin{cases} g_D(z) & \forall z \in \mathcal{N}_h \cap \Gamma_D, \\ (0,0)^{\mathrm{t}} & \forall z \in \mathcal{N}_h \setminus \Gamma_D. \end{cases} \tag{2.10}$$

Note that if g_D is not the restriction of such a function to Γ_D, $u_{0,h}|_{\Gamma_D}$ only approximates g_D. The Galerkin approximation problem is then to

$$\text{find } w_h \in \underset{\sim}{V}_h \text{ such that } a(w_h, \chi) = L(\chi) - a(u_{0,h}, \chi) \quad \forall \chi \in \underset{\sim}{V}_h, \tag{2.11}$$

giving an approximation $u_h = u_{0,h} + w_h$. The problem (2.11) also has a unique solution according to Lax-Milgram theorem applied in the Hilbert space $\left(\underset{\sim}{V}_h, (\cdot,\cdot)_{\underset{\sim}{H}^1(\Omega)}\right)$.

In subsequent chapters we will use u_h as a reference solution when we study the LOD approximation u_{LOD}. Therefore, we need to be confident that u_h approximates the exact solution u well enough. The following a priori bound tells us that this is indeed the case.

THEOREM 2.3 (error estimate for $u - u_h$ in the $\underset{\sim}{H}^1$ norm). *Let $u = u_0 + w$ and $u_h = u_{0,h} + w_h$ be the solutions corresponding to* (2.9) *and* (2.11)*, respectively. Then*

$$\|u - u_h\|_{\underset{\sim}{H}^1(\Omega)} \lesssim \inf_{\chi \in \underset{\sim}{V}_h} \|u - u_0 - \chi\|_{\underset{\sim}{H}^1(\Omega)} + \left\|u_0 - u_{0,h}\right\|_{\underset{\sim}{H}^1(\Omega)}. \tag{2.12}$$

Proof. The triangle inequality gives

$$\begin{aligned}
\|u - u_h\|_{\underset{\sim}{H}^1(\Omega)} &= \left\|u_0 + w - (u_{0,h} + w_h)\right\|_{\underset{\sim}{H}^1(\Omega)} \\
&\le \|w - w_h\|_{\underset{\sim}{H}^1(\Omega)} + \left\|u_0 - u_{0,h}\right\|_{\underset{\sim}{H}^1(\Omega)} \\
&\le \|w - \chi\|_{\underset{\sim}{H}^1(\Omega)} + \|w_h - \chi\|_{\underset{\sim}{H}^1(\Omega)} + \left\|u_0 - u_{0,h}\right\|_{\underset{\sim}{H}^1(\Omega)}
\end{aligned} \tag{2.13}$$

for some $\chi \in \underset{\sim}{V}_h$. Using (2.8) and the fact that $w_h - \chi \in \underset{\sim}{V}_h$, we can write

$$\begin{aligned}
\|w_h - \chi\|^2_{\underset{\sim}{H}^1(\Omega)} &\lesssim a(w_h - \chi, w_h - \chi) \\
&= a(w - \chi, w_h - \chi) + a(w_h - w, w_h - \chi) \\
&= a(w - \chi, w_h - \chi) + a(u_0 - u_{0,h}, w_h - \chi) \\
&\overset{(2.7)}{\lesssim} \left(\|w - \chi\|_{\underset{\sim}{H}^1(\Omega)} \|w_h - \chi\|_{\underset{\sim}{H}^1(\Omega)} + \left\|u_0 - u_{0,h}\right\|_{\underset{\sim}{H}^1(\Omega)} \|w_h - \chi\|_{\underset{\sim}{H}^1(\Omega)} \right).
\end{aligned}$$

We divide both sides by $\|w_h - \chi\|_{\underset{\sim}{H}^1(\Omega)}$ and insert the result into (2.13) to get

$$\|u - u_h\|_{\underset{\sim}{H}^1(\Omega)} \lesssim \|w - \chi\|_{\underset{\sim}{H}^1(\Omega)} + \left\|u_0 - u_{0,h}\right\|_{\underset{\sim}{H}^1(\Omega)}.$$

Since this holds for any $\chi \in \underset{\sim}{V}_h$ and $w = u - u_0$, the theorem follows. □

We can continue from (2.12) to show why the standard FEM is not suitable for the type of problem under study. Consider for simplicity the case when $\partial\Omega = \Gamma_D$, and $g_D = (0,0)^{\mathrm{t}}$ (so that $u_0 = (0,0)^{\mathrm{t}}$). Assume that $u \in \underset{\sim}{H}^2(\Omega)$ and set $\chi = \mathcal{I}_h w = \mathcal{I}_h u$, where the linear interpolation operator $\mathcal{I}_h : \underset{\sim}{\mathcal{C}}(\bar{\Omega}) \cap \underset{\sim}{H}^2(\Omega) \to \underset{\sim}{V}_h$ is defined such that $(\mathcal{I}_h u)(i) = u(i)$ for all $i \in \mathcal{N}_h$. Known interpolation error estimate $\|u - \mathcal{I}_h u\|_{\underset{\sim}{H}^1(\Omega)} \lesssim h|u|_{\underset{\sim}{H}^2(\Omega)}$ gives

$$\|u - u_h\|_{\underset{\sim}{H}^1(\Omega)} \lesssim h|u|_{\underset{\sim}{H}^2(\Omega)}. \tag{2.14}$$

This standard result is misleading for our type of problem. Firstly, the solution u might not even be a $\underset{\sim}{H}^2(\Omega)$-function and secondly, even if it is, the seemingly straightforward

estimate (2.14) is unstable in the sense that the size of $|u|_{\underset{\sim}{H}^2(\Omega)}$ is not controlled. More precisely, the rapid variations in the material parameters might carry over to the solution u, resulting in a large $|u|_{\underset{\sim}{H}^2(\Omega)}$. This may in turn result in large errors in (2.14) despite the (small) factor h. Hence, in order for the standard method to capture the behavior of the solution and yield a satisfactory approximation, h truly has to be small enough, which means that a detailed and computationally costly mesh is needed. This remark gives a better understanding of the issues with using the standard FEM and motivates the need for other methods. It is thus suitable to introduce the LOD method.

3

The local orthogonal decomposition method

As was noted earlier, the standard FEM presented in the previous section encounters difficulty in cases when data, for example material parameters, vary over several scales with many fine details. This is because in such cases a single fine mesh $\mathcal{T}_h$ needs to be able to resolve all the fine variations, creating a massive system that is costly to solve. To circumvent this problem, we now explain what has been the main focus in this thesis work, the LOD method, presented in [14] for homogeneous Dirichlet boundary value problems and later in [8] for mixed Dirichlet and Neumann boundary value problems.

To begin, we introduce a second geometrically conforming, shape regular triangulation $\mathcal{T}_H$ of Ω such that $\mathcal{T}_h$ is a refinement of $\mathcal{T}_H$. The refinement needs to include at least one uniform global refinement (i.e. a refinement of every element in $\mathcal{T}_H$). With $H_T = \operatorname{diam}(T)$ and $H = \max_{T\in\mathcal{T}_H} H_T$, we have $H \geq 2h$. We call $\mathcal{T}_H$ the coarse mesh and $\mathcal{T}_h$ the fine mesh. Similarly, we call $\underset{\sim}{V}_H = \{v \in \underset{\sim}{V} : v|_T \text{ is affine } \forall T \in \mathcal{T}_H\}$ the coarse finite element space and $\underset{\sim}{V}_h$ the fine finite element space, $\mathcal{N}_H$ the set of coarse nodes and $\mathcal{N}_h$ the set of fine nodes. Let $\mathring{\mathcal{N}}_H = \mathcal{N}_H \setminus \Gamma_D$ be the set of free coarse nodes and let $\mathring{\mathcal{N}}_h = \mathcal{N}_h \setminus \Gamma_D$ be the set of free fine nodes. Assume that Dirichlet and Neumann boundaries meet in coarse nodes, $\overline{\Gamma}_D \cap \overline{\Gamma}_N \in \mathcal{N}_H$.

The construction of the LOD method consists of two steps. In the first step, an interpolation operator is used to obtain an orthogonal splitting of the fine space $\underset{\sim}{V}_h$ into a detail space $\underset{\sim}{W}_h$ and a modified coarse space $\underset{\sim}{V}_H^{\text{ms}}$ that has good approximation properties. In the second step, the possibility to localize the splitting is utilized in order to make it less expensive to find. Afterwards, the final problem is solved in the localized modified coarse space, making it cheap.

Henceforth the standard finite element method (2.11) shall be referred to as the reference problem. The solution of the LOD method is compared to the reference solution later on, both when we perform error analysis and when we look at numerical

experiments.

3.1 Construction step 1: orthogonal decomposition

Let $\{\lambda_i\}_{i\in\mathcal{N}_H}$ be the set of coarse, piecewise linear hat functions defined by $\lambda_i(j) = \delta_{ij} \ \ \forall i,j \in \mathcal{N}_H$. In order to split the space $\underset{\sim}{V}_h$ we use a (quasi-)interpolation operator. The interpolation operator used in this thesis work is of Clément-type and is presented in [4]. It will henceforth be referred to as the Clément operator and it is defined by

$$I_H : \underset{\sim}{V} \to \underset{\sim}{V}_H, \quad v \mapsto I_H(v) = \sum_{i\in\mathring{\mathcal{N}}_H} \bar{v}(i)\lambda_i \ \text{ with } \ \bar{v}(i) = \left(\frac{(v_1,\lambda_i)}{(1,\lambda_i)}, \frac{(v_2,\lambda_i)}{(1,\lambda_i)}\right)^{\mathrm{t}}. \tag{3.1}$$

The choice of operator is not unique and a different choice might lead to a different multiscale method. The nodal values $\bar{v}(i)$ are the weighted average values of v with weights λ_i. We have the following approximation and stability properties of the Clément operator I_H [4]: for all $v \in \underset{\sim}{H}^1(\Omega)$ and for all $T \in \mathcal{T}_H$ it holds that

$$H_T^{-1}\|v - I_H v\|_T + \|\nabla(v - I_H v)\|_T \lesssim \|\nabla v\|_{\omega_T}, \tag{3.2}$$

where $\omega_T = \bigcup\{T' \in \mathcal{T}_H : T' \cap T \neq \emptyset\}$.

Define a detail space $\underset{\sim}{W}_h$ to be the kernel of I_H, i.e. $\underset{\sim}{W}_h = \{v_h \in \underset{\sim}{V}_h : I_H(v_h) = (0,0)^{\mathrm{t}}\}$. The subspace $\underset{\sim}{W}_h$ contains fine scale features of $\underset{\sim}{V}_h$ that are not captured by the coarse space $\underset{\sim}{V}_H$. It follows from Lemma 3.1 in [13] that $\underset{\sim}{V}_H$ and $\underset{\sim}{W}_h$ are orthogonal subspaces of $\underset{\sim}{V}_h$ and we can split $\underset{\sim}{V}_h$ such that

$$\underset{\sim}{V}_h = \underset{\sim}{V}_H \oplus \underset{\sim}{W}_h \quad \text{and} \quad (\underset{\sim}{V}_H, \underset{\sim}{W}_h) = 0. \tag{3.3}$$

We wish to obtain a solution space that is both low-dimensional and has good approximation properties. The coarse space $\underset{\sim}{V}_H$ fulfills the first criteria but not the second. Therefore, we need a modified coarse space that can capture details as well. Let $P_{a,h} : \underset{\sim}{V}_h \to \underset{\sim}{W}_h$ be the orthogonal projection such that for any $v_h \in \underset{\sim}{V}_h$, $P_{a,h}(v_h) \in \underset{\sim}{W}_h$ solves

$$a(P_{a,h}(v_h), \chi) = a(v_h, \chi) \ \ \forall \chi \in \underset{\sim}{W}_h. \tag{3.4}$$

Hence $P_{a,h}(v_h)$ is the best approximation of v_h in $\underset{\sim}{W}_h$ with respect to the inner product $a(\cdot,\cdot)$. Note that $(1 - P_{a,h})(\underset{\sim}{V}_h) = (1 - P_{a,h})(\underset{\sim}{V}_H)$ since $(1 - P_{a,h})(\underset{\sim}{W}_h) = 0$. From this we define the modified coarse space

$$\underset{\sim}{V}_H^{\mathrm{ms}} = (1 - P_{a,h})(\underset{\sim}{V}_H), \tag{3.5}$$

which contains fine scale information due to $P_{a,h}$. By Lemma 3.2 in [13] we then split $\underset{\sim}{V}_h$ such that

$$\underset{\sim}{V}_h = \underset{\sim}{V}_H^{\mathrm{ms}} \oplus \underset{\sim}{W}_h \quad \text{and} \quad a(\underset{\sim}{V}_H^{\mathrm{ms}}, \underset{\sim}{W}_h) = 0. \tag{3.6}$$

Consequently, any function $u_h \in \underset{\sim}{V}_h$ can be decomposed into $u_h = u_H^{\mathrm{ms}} + u^f$, where $u_H^{\mathrm{ms}} \in \underset{\sim}{V}_H^{\mathrm{ms}}$, $u^f \in \underset{\sim}{W}_h$ and $a(u_H^{\mathrm{ms}}, u^f) = 0$. Note that

$$\dim(\underset{\sim}{V}_H^{\mathrm{ms}}) = \dim(\underset{\sim}{V}_h) - \dim(\underset{\sim}{W}_h) = \dim(\underset{\sim}{V}_H).$$

The projection $P_{a,h}$ can be expressed as $P_{a,h} = \sum_{T\in\mathcal{T}_H} Q_h^T$, where $Q_h^T : \underset{\sim}{V}_h \to \underset{\sim}{W}_h$ is the operator such that for any $v_h \in \underset{\sim}{V}_h$, $Q_h^T(v_h) \in \underset{\sim}{W}_h$ solves

$$a\left(Q_h^T(v_h), \chi\right) = a(v_h, \chi)_T \quad \forall \chi \in \underset{\sim}{W}_h. \tag{3.7}$$

We call Q_h^T a corrector operator and (3.7) the corresponding corrector problem.

3.2 Construction step 2: localization of the splitting

We have obtained a modified coarse space $\underset{\sim}{V}_H^{\text{ms}}$ in which we can look for an approximation of the solution of the elastcity problem. Since $\underset{\sim}{V}_H^{\text{ms}}$ is low-dimensional compared to $\underset{\sim}{V}_h$, the problem is cheaper. However, it is expensive to find the exact splitting $\underset{\sim}{V}_h = \underset{\sim}{V}_H^{\text{ms}} \oplus \underset{\sim}{W}_h$ since this involves solving large corrector problems (3.7). It turns out that this setback can be redeemed since $Q_h^T(v_h)$ decays exponentially to zero outside of T. Because of this property, the corrector problems (and consequently, the detail space $\underset{\sim}{W}_h$) can be localized, restricted to, and solved over small patches around their corresponding elements instead of over the entire domain. It is rather technical to show this exponential decay property and we refer to Appendix A in [8] for a complete proof of it. The setting in [8] is not identical to ours, but the same property can be expected for our elasticity problem as well.

In order to localize the fine scale computations we define patches as follows.

Definition 3.1 (element patch). *Let $k \in \mathbb{N}$ and $T \in \mathcal{T}_H$. An element patch $U_k(T)$ around T is a subset of the coarse mesh $\mathcal{T}_H$ such that*

$$U_k(T) = \begin{cases} T & \text{if } k = 0, \\ \bigcup\{T' \in \mathcal{T}_H : T' \cap U_{k-1}(T) \neq \emptyset\} & \text{if } k = 1, 2, \dots \end{cases} \tag{3.8}$$

The indicator $k = k(T)$ is referred to as the patch size or the number of layers of $U_k(T)$.

As k increases we eventually end up with $U_k(T) = \Omega$. Note that the sizes of the element patches may vary for different T. Patches do not necessarily have to align with the coarse mesh $\mathcal{T}_H$ for the LOD method to work, but we define the patches in this way because these are the only types of patches that are used in our implementation. We collect all element patches in the set

$$\mathcal{U} = \{U_k(T) : T \in \mathcal{T}_H \text{ and } U_k(T) \text{ is an element patch}\},$$

where $\mathcal{U}$ contains one and only one element patch for each T. Let $\overset{\circ}{\underset{\sim}{W}}_h(U_k(T)) = \{w_h \in \underset{\sim}{W}_h : w_h = 0 \text{ in } \Omega \setminus U_k(T)\}$ be the restriction of $\underset{\sim}{W}_h$ to $U_k(T)$.

Now that we have explained what we mean by localization and have defined element patches, we can define the LOD method for solving the elasticity problem. The definition is similar to the one given in [8].

DEFINITION 3.2 (LOD approximation for boundary value problems). *For a given set $\mathcal{U}$ of element patches, we define the local corrector operator $Q_h^T : \underset{\sim}{V}_h \to \mathring{\underset{\sim}{W}}_h(U_k(T))$ by the following: for a given $\phi_h \in \underset{\sim}{V}_h$ and $T \in \mathcal{T}_H$, find $Q_h^T(\phi_h) \in \mathring{\underset{\sim}{W}}_h(U_k(T))$ such that*

$$a\left(Q_h^T(\phi_h), w_h\right) = a(\phi_h, w_h)_T \quad \forall w_h \in \mathring{\underset{\sim}{W}}_h(U_k(T)). \tag{3.9}$$

The Neumann boundary correctors are given by the following: for all $T \in \mathcal{T}_H$ with $T \cap \Gamma_N \neq \emptyset$, find $B_h^T \in \mathring{\underset{\sim}{W}}_h(U_k(T))$ such that

$$a(B_h^T, w_h) = \int_{T\cap\Gamma_N} g_N \cdot w_h \,\mathrm{d}s \quad \forall w_h \in \mathring{\underset{\sim}{W}}_h(U_k(T)). \tag{3.10}$$

The global correctors are given by

$$Q_h(\phi_h) = \sum_{T\in\mathcal{T}_H} Q_h^T(\phi_h) \;\text{ and }\; B_h = \sum_{\substack{T\in\mathcal{T}_H \\ T\cap\Gamma_N\neq\emptyset}} B_h^T. \tag{3.11}$$

Defining $R_h = Id - Q_h$, the LOD approximation is given by $u_{\mathrm{LOD}} = R_h(v_H + u_{0,h}) + B_h$, where $v_H \in \underset{\sim}{V}_H$ solves

$$a\left(R_h(v_H), R_h(\Phi_H)\right) = L\left(R_h(\Phi_H)\right) - a\left(R_h(u_{0,h}) + B_h, R_h(\Phi_H)\right) \;\; \forall \Phi_H \in \underset{\sim}{V}_H. \tag{3.12}$$

We call (3.12) *the multiscale problem and $Q_h(u_{0,h})$ the global Dirichlet boundary corrector.*

Let $\underset{\sim}{V}_{H,k}^{\mathrm{ms}} = \{R_h(\Phi_H) : \Phi_H \in \underset{\sim}{V}_H\}$ denote the localized multiscale space. The multiscale problem (3.12) has a unique solution according to Lax-Milgram theorem applied in the Hilbert space $\left(\underset{\sim}{V}_{H,k}^{\mathrm{ms}}, (\,\cdot\,,\cdot\,)_{\underset{\sim}{H}^1(\Omega)}\right)$. Note that u_{LOD} does not necessarily lie in $\underset{\sim}{V}_{H,k}^{\mathrm{ms}}$.

At a first glance, it might look like an intimidating task to find the LOD approximation from Definition 3.2. We have to account for the mixed boundary conditions and we need to compute correctors. This task becomes clearer in the next chapter, where we describe how an LOD solver for the elasticity problem is implemented. We may also compare the multiscale problem (3.12) with the standard finite element problem, our reference problem (2.11), and find similarities in their forms.

4

Implementation of LOD solver

In this chapter we describe how an LOD solver of the elasticity problem is implemented. The first section presents some preliminaries for solving the problem. As a first step in the actual implementation process, a standard finite element solver was implemented. This step was facilitated by [11], as this book provided some helpful code. This step also resulted in a full understanding of the assembly process, which is identical for both solvers. The solvers were implemented in MATLAB.

Not only can a standard finite element solver be used to obtain u_h, but it can also be used to check the correctness of an LOD solver. More specifically, if we have a homogeneous $\Gamma_D = \partial\Omega$, a body load $f \in \underset{\sim}{V}_H$, and $U_k(T) = \Omega \ \ \forall T \in \mathcal{T}_H$, the standard FEM and the LOD method have the same solution and hence the two solvers should give the same answer. To see this, begin with the multiscale problem, which in this case becomes

$$a(u_{\text{LOD}}, \Phi) = (f, \Phi) \ \ \forall \Phi \in \underset{\sim}{V}_H^{\text{ms}}. \tag{4.1}$$

Now, $a(u_{\text{LOD}}, \varphi^f) = 0 \ \ \forall \varphi^f \in \underset{\sim}{W}_h$ by (3.6) and $(f, \varphi^f) = 0 \ \ \forall \varphi^f \in \underset{\sim}{W}_h$ by (3.3). Defining $\chi = \Phi + \varphi^f \in \underset{\sim}{V}_h$, (4.1) can thus be rewritten as

$$a(u_{\text{LOD}}, \chi) = (f, \chi) \ \ \forall \chi \in \underset{\sim}{V}_h,$$

and this problem is identical to the standard finite element problem.

The second section describes how the corrector problems (3.9) and (3.10) are solved in practice.

4.1 Preliminaries: assembly of stiffness matrix and load vector

In general, when implementing a finite element solver of a partial differential equation, the weak formulation is translated into a linear system of equations

$$Kd = F, \tag{4.2}$$

where K is called the stiffness matrix, F is called the load vector, and d is the solution of the system. In our case, the solution is a nodal displacement vector. Both K and F are assembled by looping over the triangles in $\mathcal{T}_h$ and storing the contributions from each triangle in an ordered way. Since the solution of the two-dimensional elasticity problem is a displacement vector $u = (u_1, u_2)^{\mathrm{t}}$, a node $N_i \in \mathcal{N}_h$ is made up of two degrees of freedom (DOFs), one for the horizontal displacement and one for the vertical displacement. Therefore, we express the finite element solution $u_h = (u_{h,1}, u_{h,2})^{\mathrm{t}}$ as

$$u_h = \varphi d = \begin{pmatrix} \varphi_1 & 0 & \varphi_2 & 0 & \dots & \varphi_n & 0 \\ 0 & \varphi_1 & 0 & \varphi_2 & \dots & 0 & \varphi_n \end{pmatrix} \begin{pmatrix} d_{11} \\ d_{12} \\ d_{21} \\ d_{22} \\ \vdots \\ d_{n1} \\ d_{n2} \end{pmatrix}, \tag{4.3}$$

where $\{\varphi_i\}_{i \in \mathcal{N}_h}$ is the set of fine, piecewise linear hat functions defined by $\varphi_i(j) = \delta_{ij} \ \ \forall i, j \in \mathcal{N}_h$. There are two displacement values d_{i1} and d_{i2} per node i or, equivalently, one displacement value per DOF. Henceforth, we generally use the notation $d(v_h)$ for the (fine) nodal displacement vector corresponding to the function $v_h \in \underset{\sim}{V}_h$.

Going from (2.11) to (4.2) is straightforward but quite lengthy. We therefore refer to [11] for a detailed description of the translation, while merely stating the results here. Consider some $T \in \mathcal{T}_h$ having nodes i, j, and k as vertices. Let φ_i, φ_j and φ_k be the corresponding hat functions. We get an element stiffness matrix

$$K^T = \int_T S^{T\mathrm{t}} \, D^T \, S^T \, \mathrm{d}x \tag{4.4}$$

and an element load vector

$$F^T = \int_T \varphi^{T\mathrm{t}} \, f \, \mathrm{d}x + \int_{\partial T \cap \Gamma_N} \varphi^{T\mathrm{t}} \, g_N \, \mathrm{d}s, \tag{4.5}$$

where

$$S^T = \begin{pmatrix} \partial/\partial x & 0 \\ 0 & \partial/\partial y \\ \partial/\partial y & \partial/\partial x \end{pmatrix} \varphi^T = \begin{pmatrix} \partial/\partial x & 0 \\ 0 & \partial/\partial y \\ \partial/\partial y & \partial/\partial x \end{pmatrix} \begin{pmatrix} \varphi_i & 0 & \varphi_j & 0 & \varphi_k & 0 \\ 0 & \varphi_i & 0 & \varphi_j & 0 & \varphi_k \end{pmatrix}$$

is the element strain matrix and

$$D^T = \begin{pmatrix} \lambda + 2\mu & \lambda & 0 \\ \lambda & \lambda + 2\mu & 0 \\ 0 & 0 & \mu \end{pmatrix}$$

is the elasticity matrix that relates to Hooke's law (2.3b). The integrals in (4.4) and (4.5) are computed with some quadrature rule. If the Lamé parameters are constant over an element, the integrand in (4.4) is constant as well. The global stiffness matrix $K = \sum_{T\in\mathcal{T}_h} K^T$ and global load vector $F = \sum_{T\in\mathcal{T}_h} F^T$ are then obtained by assembling K^T and F^T according to a map that ensures that the contributions are added correctly. Since there are n nodes in the triangulation, K and F are $2n\times 2n$ and $2n\times 1$, respectively.

The nodes lying on Γ_D are called fixed nodes or Dirichlet nodes and the remaining nodes are called free nodes. In order to handle the possibly inhomogeneous Dirichlet boundary condition that manifests itself in the finite element problem (2.11), the system (4.2) needs to be modified slightly by separating the free parts of the matrices from the fixed parts. If m out of n nodes are free, then the free parts K_{ff} and F_f are $2m \times 2m$ and $2m \times 1$, respectively, and the modified linear system becomes

$$\begin{pmatrix} K_{ff} & K_{fD} \\ 0 & I \end{pmatrix} \begin{pmatrix} d_f \\ d_D \end{pmatrix} = \begin{pmatrix} F_f \\ F_D \end{pmatrix}.$$

From this system the fixed part of the solution follows immediately because F_D is just a vector with the nodal values of g_D. Therefore, we can solve $K_{ff}d_f = F_f - K_{fD}d_D$ in the way described above and simply add the fixed part d_D of the solution afterwards. When the nodal displacement vector d has been computed, u_h is obtained immediately from (4.3) (the odd elements in d give the first component of u_h and the even elements in d give the second component).

4.2 Solving localized corrector problems and obtaining a basis of the localized multiscale space

We now return to Defintion 3.2 and explain how it is used to compute the LOD approximation. We begin by mentioning how the local corrector problems are solved in practice. A routine that extracts element patches is required. Such a routine was made available from previous work. Given an element patch $U_k(T)$, let $\underset{\sim}{\overset{\circ}{V}}_h(U_k(T)) = \{v_h \in \underset{\sim}{V}_h : v_h = 0 \text{ in } \Omega \setminus U_k(T)\}$ be the restriction of $\underset{\sim}{V}_h$ to $U_k(T)$. In order to assemble the corrector problem (3.9) (and, similarly, (3.10)) we need the test function w_h and trial function $Q_h^T(\phi_h)$ to lie in $\underset{\sim}{\overset{\circ}{V}}_h$ rather than $\underset{\sim}{\overset{\circ}{W}}_h$. Therefore, we reformulate (3.9) in the following way: given $\phi_h \in \underset{\sim}{V}_h$ and $T \in \mathcal{T}_H$, find $Q_h^T(\phi_h) \in \underset{\sim}{\overset{\circ}{V}}_h$ such that

$$\begin{aligned} &a(Q_h^T(\phi_h), w_h) = a(\phi_h, w_h)_T \quad \forall w_h \in \underset{\sim}{\overset{\circ}{V}}_h(U_k(T)) \\ &\text{s.t} \quad I_H(w_h) = 0, \\ &\qquad I_H\left(Q_h^T(\phi_h)\right) = 0. \end{aligned} \tag{4.6}$$

When written on this form, Lagrange multipliers can be used to translate the local corrector problem into a system of equations. This system contains a localized stiffness matrix, assembled on the patch $U_k(T)$ according to the previous section, and the Clément

operator from (3.1), localized to the patch $U_k(T)$. Since $I_H : \underset{\sim}{V}_h \to \underset{\sim}{V}_H$, the localized Clément operator is represented by a $2N_H$–by–$2N_h$ matrix in MATLAB, where N_H and N_h are the number of free coarse nodes and free fine nodes in $U_k(T)$, respectively. The factor 2 enters since there are two DOFs per node. A MATLAB function that computes the Clément matrix was made available from previous work. Collecting the Lagrange multipliers in μ, the system of equations corresponding to (3.9) becomes

$$\begin{pmatrix} K^{U_k(T)} & (I_H)^{\mathrm{t}} \\ I_H & 0 \end{pmatrix} \begin{pmatrix} d\left(Q_h^T(\phi_h)\right) \\ \mu \end{pmatrix} = \begin{pmatrix} K^T d(\phi_h) \\ 0 \end{pmatrix} \tag{4.7}$$

The system that corresponds to (3.10) follows analogously. The exact reasoning in going from (4.6) to (4.7) is not included here since it tends towards optimization theory. Given ϕ_h, the system (4.7) can be solved in MATLAB to obtain the local corrector $Q_h^T(\phi_h)$.

Global correctors as those in (3.11) are computed by looping over the coarse triangles in $\mathcal{T}_H$ and solving local corrector problems (3.9) and (3.10) in each iteration. It is simple to find the Dirichlet corrector $Q_h(u_{0,h})$ and the Neumann corrector B_h since the boundary conditions $u_{0,h}|_{\Gamma_D}$ and g_N are known. Note that a local Dirichlet corrector problem (3.9) needs to be solved only if the element T shares an edge with Γ_D.

We need to make an important remark about notation and how functions in $\underset{\sim}{V}_h$ can be written. Consider the displacement vector d from the previous section. Let $\mathcal{D}_h$ denote the set of fine DOFs. The number of fine DOFs is $|\mathcal{D}_h| = 2|\mathcal{N}_h|$. One displacement value is assigned for each fine DOF and we see that the displacement can be represented by a scalar valued function

$$u_h = \sum_{i \in \mathcal{D}_h} d_i \varphi_i, \tag{4.8}$$

where $\{\varphi_i\}_{i \in \mathcal{D}_h}$ is the set of fine hat functions defined by the DOFs rather than the nodes. In the standard finite element method, the representation of u_h as a scalar valued function is unnecessary since (4.2) gives us the displacement values directly, and we can immediately obtain u_h as in (4.3). In the LOD method, on the other hand, we look for an approximation in a modified, low dimensional space. Therefore, we have to obtain a multiscale basis and perform a change of basis for the stiffness matrix and load vector before we can solve the multiscale problem (3.12). Then we need to write the LOD approximation u_{LOD} explicitly in terms of this multiscale basis in the same way u_h is written in terms of $\{\varphi_i\}_{i \in \mathcal{D}_h}$ in (4.8). In order to give a proper review of this procedure we will allow a twofold representation of functions in $\underset{\sim}{V}_h$. These functions are vector valued, characterized by the nodes $\mathcal{N}_h$, but they can also be considered as scalar valued functions, characterized by the DOFs in $\mathcal{D}_h$ (for instance, compare u_h in (4.3) with u_h in (4.8)). The secondary representation leads to a slight misuse of notation since we have defined the LOD method for vector valued functions.[1] This is acceptable because the new way of representing functions in $\underset{\sim}{V}_h$ is crucial in order to give a convenient description of the implementation, but also in order to perform the analysis in the next

[1] The LOD method could have been defined for scalar valued functions in order to avoid this misuse. However, we wanted to be consistent in our formulations of the standard FEM and the LOD method.

chapter. Effectively, there is no difference between the two representations since both are defined by the $|\mathcal{D}_h| = 2|\mathcal{N}_h|$ values in the displacement vector. With this remark, we are able to find the multiscale basis of $\underset{\sim}{V}{}^{\text{ms}}_{H,k}$.

Let $\mathcal{D}_H$ and $\mathring{\mathcal{D}}_H$ denote the set of coarse DOFs and set of free coarse DOFs, respectively. Let $\{\lambda_i\}_{i\in\mathcal{D}_H}$ be the set of coarse, piecewise linear hat functions defined by $\lambda_i(j) = \delta_{ij} \quad \forall i, j \in \mathcal{D}_H$. See Figures 4.1(a)-(b) for an example of a λ_j. The functions λ_{2i-1} and λ_{2i} both take the value 1 at node i but they are not equal. For instance, had we instead plotted λ_{j+1}, the hat would have been in the right figure instead (assuming j is odd).

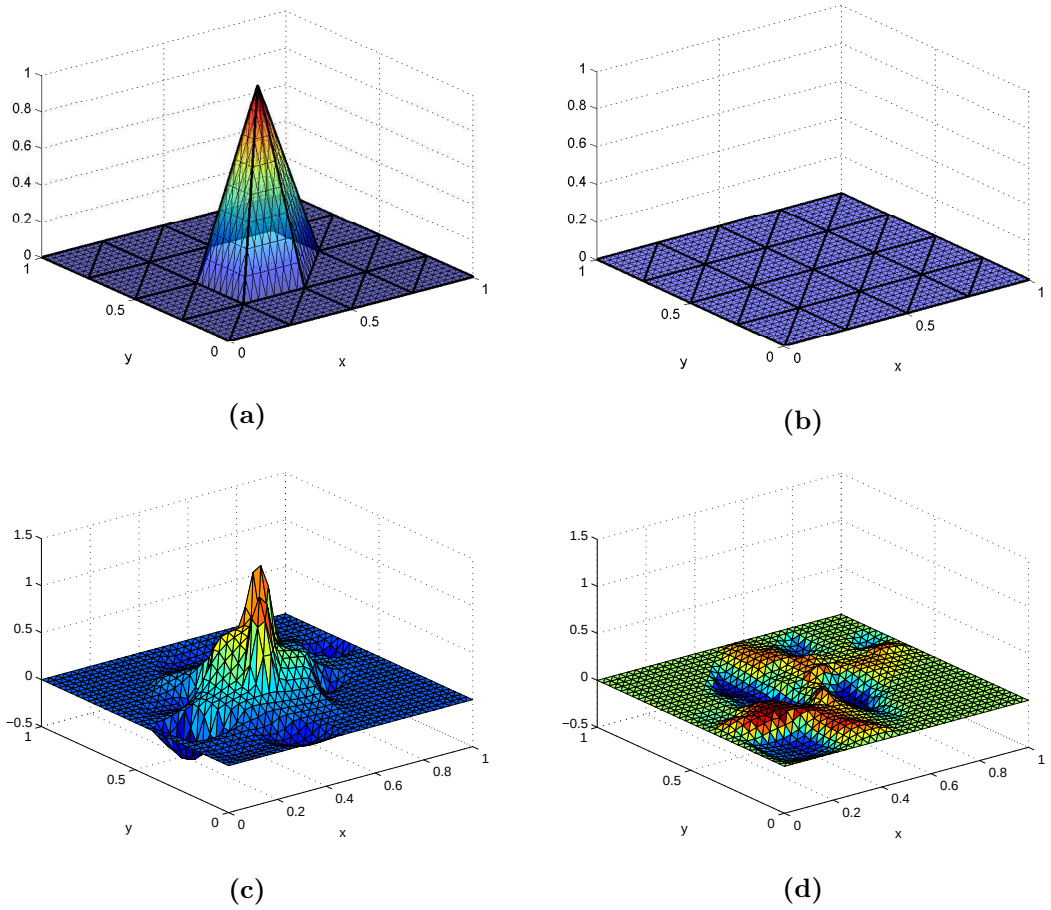

Figure 4.1. The difference between basis functions. (a) and (b) show a coarse hat function $\lambda_j \in \underset{\sim}{V}_H$ on $\Omega = (0,1) \times (0,1)$, where $H = 2^{-2}$ and j is located at $(0.5, 0.5)^{\text{t}}$. (c) and (d) show a corresponding modified basis function $\lambda_j - \theta_j \in \underset{\sim}{V}{}^{\text{ms}}_{H,k}$ for some problem, where $k = 1$ and the fine mesh size $h = 2^{-5}$. The modified basis function captures fine scale details and is problem dependent, as can be understood from (3.5). Note that the support of $\lambda_j - \theta_j$ is $\bigcup_{T\in\text{supp}(\lambda_j)} U_1(T)$, which illustrates the final equality in (4.11).

We proceed by solving corrector problems (3.9) for these hat functions. A given $T \in \mathcal{T}_H$ lies in the support of six coarse hat functions. Call them λ_{2i-1}, λ_{2i}, λ_{2j-1}, λ_{2j}, λ_{2k-1} and λ_{2k}. For each T, we solve the local corrector problem (3.9) four times, for $\phi_h = \lambda_{2i-1}$, λ_{2i}, λ_{2j-1}, λ_{2j} (i.e., we extrapolate the functions and solve (4.7) four times). The fifth and sixth corrector, $Q_h^T(\lambda_{2k-1})$ and $Q_h^T(\lambda_{2k})$, can be obtained from the other four since the hat functions have a partition of unity property. More specifically,

$$a\left(Q_h^T(\lambda_{2i}) + Q_h^T(\lambda_{2j}) + Q_h^T(\lambda_{2k}), w_h\right) = a(\lambda_{2i} + \lambda_{2j} + \lambda_{2k}, w_h)_T = a(1, w_h)_T = 0$$

for all $w_h \in \mathring{\underset{\sim}{W}}_h(U_k(T))$, giving $Q_h^T(\lambda_{2k}) = -Q_h^T(\lambda_{2i}) - Q_h^T(\lambda_{2j})$. It is of course more efficient to solve four corrector problems instead of six. When the local correctors have been computed, the ones obtained from free DOFs are added to their corresponding global correctors. For instance, we can see that the free DOF j in Figure 4.1(a) is involved in six local corrector problems and thus the global corrector corresponding to this DOF is a sum of six local correctors. Denoting the global correctors θ_i, $i \in \mathring{\mathcal{D}}_H$, we obtain a multiscale basis

$$\{\lambda_i - \theta_i\}_{i \in \mathring{\mathcal{D}}_H}$$

of $\underset{\sim}{V}_{H,k}^{\text{ms}}$. See Figures 4.1(c)-(d) for an example of what a modified basis function may look like.

We can now solve the multiscale problem (3.12) in MATLAB by changing to the multiscale basis for the matrices assembled in the previous section. More specifically, let B denote the change of basis matrix

$$B = \begin{pmatrix} d(\lambda_1 - \theta_1) & d(\lambda_2 - \theta_2) & \dots & d(\lambda_{|\mathring{\mathcal{D}}_H|} - \theta_{|\mathring{\mathcal{D}}_H|}) \end{pmatrix}.$$

Then the multiscale system of equations becomes

$$\left(B^{\text{t}} K_{ff} B\right) \alpha = B^{\text{t}}(F_f - K_{fD} d_D) + B^{\text{t}} K_{ff}\, d\left(Q_h(u_{0,h})\right) - B^{\text{t}} K_{ff}\, d(B_h). \tag{4.9}$$

The solution is a vector α that defines $R_h(v_H)$. Hence, this part of the LOD approximation can now be written as

$$R_h(v_H) = \sum_{i \in \mathring{\mathcal{D}}_H} \alpha_i(\lambda_i - \theta_i). \tag{4.10}$$

Finally, we obtain the LOD approximation $u_{\text{LOD}} = R_h(v_H + u_{0,h}) + B_h$ by adding the fixed part of the solution (i.e. the part on the Dirichlet boundary) and the two global boundary correctors.

The right hand side of (4.10) can be expanded to give an expression of $R_h(v_H)$ in terms of the elements in $\mathcal{T}_H$. We have

$$R_h(v_H) = \sum_{i \in \mathring{\mathcal{D}}_H} \alpha_i(\lambda_i - \theta_i) = \sum_{i \in \mathring{\mathcal{D}}_H} \alpha_i \left(\lambda_i - \sum_{T \in \text{supp}(\lambda_i)} Q_h^T(\lambda_i)\right)$$

$$= \sum_{i \in \mathring{\mathcal{D}}_H} \alpha_i \sum_{T \in \mathrm{supp}(\lambda_i)} (\lambda_i^T - q_i^T) = \sum_{i \in \mathring{\mathcal{D}}_H} \sum_{T \in \mathcal{T}_H} \alpha_i (\lambda_i^T - q_i^T), \tag{4.11}$$

where λ_i^T coincides with λ_i on T but is zero elsewhere. We have set $Q_h^T(\lambda_i) = Q_h^T(\lambda_i^T) = q_i^T$ in order to simplify the notation. The final equality in (4.11) holds because if i is given, then λ_i^T is zero when $T \notin \mathrm{supp}(\lambda_i)$ (and when λ_i^T is zero on some T, the corresponding local corrector q_i^T is zero as well). By rearranging the summations in (4.11), we note that $R_h(v_H)$ can also be expressed as

$$R_h(v_H) = \sum_{T \in \mathcal{T}_H} \sum_{i \in \mathring{\mathcal{D}}_H} \alpha_i (\lambda_i^T - q_i^T) = \sum_{T \in \mathcal{T}_H} \sum_{i \in \mathring{\mathcal{D}}_H \cap T} \alpha_i (\lambda_i^T - q_i^T), \tag{4.12}$$

where the final equality holds because given T, λ_i^T is zero if the DOF i is not on a vertex of T (and when λ_i^T is zero for some i, the corresponding local corrector q_i^T is zero as well). In the homogeneous Dirichlet problem both the fixed part and the correctors are zero. In this case we have $u_{\mathrm{LOD}} = R_h(v_H)$. The expression (4.12) will be utilized in the next section when we prove an a posteriori error estimate for our elasticity problem.

5

A posteriori error estimate for the homogeneous Dirichlet problem

In this chapter we prove an a posteriori error estimate for the LOD method. Generally, an a posteriori error estimate is expressed in terms of the computed solution rather than the exact solution. The idea is to find an estimate that depends on residuals computed on elements in $\mathcal{T}_H$. It is then possible to find the elements that contribute the most to the error. This allows for an adaptive algorithm that reduces the large residuals by modifying the settings of the method. A basic adaptive algorithm is proposed in Section 5.1.

For $T \in \mathcal{T}_H$, define the cutoff function $\eta_k^T \in \underset{\sim}{V}_H$ such that

$$\eta_k^T(j) = \begin{cases} (0,0)^{\mathrm{t}} & \forall j \in \mathcal{N}_H \cap U_{k-1}(T), \\ (1,1)^{\mathrm{t}} & \forall j \in \mathcal{N}_H \cap \left(\Omega \setminus U_{k-1}(T)\right), \end{cases} \tag{5.1}$$

and $\left\|\nabla \eta_k^T\right\|_{\underset{\sim}{L}^\infty\left(U_k(T)\setminus U_{k-1}(T)\right)} \lesssim H^{-1}$. Recall the inequality (3.2). Some additional results associated with the Clément operator are given in the following lemma.

LEMMA 5.1. *For all $v_H \in \underset{\sim}{V}_H$ there exists a $v_h \in \underset{\sim}{V}_h$ with*

$$I_H(v_h) = v_H, \quad \|\nabla v_h\| \lesssim \|\nabla v_H\| \quad \textit{and} \quad \operatorname{supp}(v_h) \subset \operatorname{supp}(v_H).$$

For a proof, see Lemma 2.1 in [14]. With this lemma in our arsenal, we are ready to prove the main theorem of this thesis.

THEOREM 5.2 (a posteriori error estimate for the LOD method). *Consider the elasticity problem* (2.3) *in the case when $\Gamma_D = \partial\Omega$ and $g_D = (0,0)^{\mathrm{t}}$. Let u_h be the solution of the*

reference problem (2.11) *and let* u_{LOD} *be the LOD approximation from Definition 3.2. Then we have the following a posteriori error estimate:*

$$|||u_h - u_{\mathrm{LOD}}||| \lesssim K\left[\sum_{T\in\mathcal{T}_H} H_T^2\|f\|_T^2\right]^{1/2} + K^{3/2}\left[\sum_{T\in\mathcal{T}_H} |||u_{\mathrm{LOD}}^T|||^2_{U_k(T)\setminus U_{k-3}(T)}\right]^{1/2}, \quad (5.2)$$

where $u_{\mathrm{LOD}}^T = \sum_{i\in\mathring{\mathcal{D}}_H\cap T}\alpha_i(\lambda_i^T - q_i^T)$ *and* $K = \max_{T\in\mathcal{T}_H} k(T)$ *is the size of the biggest element patch in* $\mathcal{U}$*.*

Proof. Define $e_h = u_h - u_{\mathrm{LOD}} \in \underset{\sim}{V}_h$, where $u_h \in \underset{\sim}{V}_h$ is the unique solution of the problem $a(u_h,\chi) = (f,\chi) \ \ \forall\chi\in\underset{\sim}{V}_h$ and $u_{\mathrm{LOD}} \in \underset{\sim}{V}{}^{\mathrm{ms}}_{H,k}$ is the unique solution of the problem $a(u_{\mathrm{LOD}},\Phi) = (f,\Phi) \ \ \forall\Phi\in\underset{\sim}{V}{}^{\mathrm{ms}}_{H,k}$. By Galerkin orthogonality it follows that $a(u_h - u_{\mathrm{LOD}},\Phi) = 0 \ \ \forall\Phi\in\underset{\sim}{V}{}^{\mathrm{ms}}_{H,k}$. In order to utilize the Galerkin orthogonality in the proof, we need to find an interpolant of e_h in $\underset{\sim}{V}{}^{\mathrm{ms}}_{H,k}$. To this end, let $P_H : \underset{\sim}{V}_h \to \underset{\sim}{V}_H$ be the orthogonal projection such that for any $v_h \in \underset{\sim}{V}_h$, $P_H v_h \in \underset{\sim}{V}_H$ solves

$$(P_H v_h,\chi) = (v_h,\chi) \ \ \forall\chi\in\underset{\sim}{V}_h. \quad (5.3)$$

With this projection we define an interpolant

$$e_{H,k}^c = (1-Q_h)P_H e_h = R_h(P_H e_h) \in \underset{\sim}{V}{}^{\mathrm{ms}}_{H,k}.$$

Now,

$$\begin{aligned}|||e_h|||^2 &= a(e_h,e_h) = a(u_h, e_h - e_{H,k}^c) - a(u_{\mathrm{LOD}}, e_h - e_{H,k}^c)\\ &= \underbrace{a(u_h, e_h - e_{H,k}^c)}_{=\mathrm{I}} + \underbrace{a(u_{\mathrm{LOD}}, e_{H,k}^c - e_h)}_{=\mathrm{II}}. \end{aligned} \quad (5.4)$$

One important observation to make is that $e_h - e_{H,k}^c \in \underset{\sim}{W}_h = \{v\in\underset{\sim}{V} : I_H(v) = (0,0)^{\mathrm{t}}\}$. It follows from the fact that $P_H = \left(I_H|_{\underset{\sim}{V}_H}\right)^{-1} I_H$, and, consequently, $I_H(e_h - e_{H,k}^c) = I_H e_h - I_H P_H e_h = (0,0)^{\mathrm{t}}$. See Remark 3.1 in [13] for more details.

For the first term in (5.4) we have

$$\begin{aligned}\mathrm{I} &= a\left(u_h, e_h - e_{H,k}^c\right) = (f, e_h - e_{H,k}^c)\\ &= \sum_{T\in\mathcal{T}_H}\left(f, e_h - e_{H,k}^c\right)_T\\ &\le \sum_{T\in\mathcal{T}_h}\|f\|_T\left\|e_h - e_{H,k}^c\right\|_T\\ &\overset{(3.2)}{\lesssim} \sum_{T\in\mathcal{T}_H} H_T\|f\|_T\,|||e_h - e_{H,k}^c|||_{U_1(T)}\\ &\overset{\mathrm{CS}}{\lesssim} |||e_h - e_{H,k}^c|||\left[\sum_{T\in\mathcal{T}_H} H_T^2\|f\|_T^2\right]^{1/2}, \end{aligned} \quad (5.5)$$

with CS indicating the use of the Cauchy-Schwarz inequality. We wish to find an upper bound of $|||e_h - e^c_{H,k}|||$ in terms of $|||e_h|||$. The triangle inequality gives

$$|||e_h - e^c_{H,k}||| \leq |||e_h||| + |||P_H e_h||| + |||Q_h P_H e_h|||. \tag{5.6}$$

For any $v \in \underset{\sim}{V}_h$,

$$|||Q_h v|||^2 = a\left(\sum_{T\in\mathcal{T}_H} Q_h^T v, \sum_{S\in\mathcal{T}_H} Q_h^S v\right) = \sum_{T\in\mathcal{T}_H} \sum_{S\in U_{k(T)+K}(T)} a(Q_h^T v, Q_h^S v).$$

The summation over S can be modified in this way because for a given T, $Q_h^T v \in \mathring{\underset{\sim}{W}}_h(U_k(T))$ and therefore $a(Q_h^T v, Q_h^S v)$ is zero if $U_k(T) \cap U_k(S) = \emptyset$. We replace $k(T)$ with K and continue,

$$\begin{aligned}|||Q_h v|||^2 &\leq \sum_{T\in\mathcal{T}_h} \sum_{S\in U_{2K}(T)} |||Q_h^T v|||||Q_h^S v||| \overset{(3.9)}{\leq} \sum_{T\in\mathcal{T}_h} \sum_{S\in U_{2K}(T)} |||v|||_T |||v|||_S \\ &\lesssim \sum_{T\in\mathcal{T}_h} \sum_{S\in U_{2K}(T)} |||v|||_T^2 + |||v|||_S^2 \lesssim \sum_{T\in\mathcal{T}_h} K^2 |||v|||_T^2 + |||v|||_{U_{2K}(T)}^2 \lesssim K^2 |||v|||^2. \end{aligned} \tag{5.7}$$

When we sum over S in (5.7), K enters because the number of elements in a patch grows roughly quadratically with K and can be bounded by $C_p K^2$. When we sum over T in (5.7), K enters because the number of patches that overlap a single element can be bounded analogously.

$\mathcal{T}_H$ is shape-regular in the sense of [1] and the result in this paper gives us the stability estimate $|||P_H e_h||| \lesssim |||e_h|||$. This estimate together with (5.6) and (5.7) give

$$|||e_h - e^c_{H,k}||| \lesssim |||e_h||| + K|||e_h||| \lesssim K|||e_h|||. \tag{5.8}$$

By inserting (5.8) into (5.5) we get

$$\mathrm{I} \lesssim K|||e_h|||\left[\sum_{T\in\mathcal{T}_H} H_T^2 \|f\|_T^2\right]^{1/2}. \tag{5.9}$$

Now turn the attention to the second term in (5.4). Set $\epsilon = e^c_{H,k} - e_h \in \underset{\sim}{W}_h$. We use (4.12) and recall that $a(\lambda_i^T, w^T)_T - a(q_i^T, w^T) = 0$ for all $w^T \in \mathring{\underset{\sim}{W}}_h(U_k(T))$ according to (3.9), where $q_i^T = Q_h^T(\lambda_i^T)$, to get

$$\begin{aligned}\mathrm{II} = a(u_{\mathrm{LOD}}, \epsilon) &= a\left(\sum_{T\in\mathcal{T}_H} \sum_{i\in\mathring{\mathcal{D}}_H\cap T} \alpha_i(\lambda_i^T - q_i^T),\ \epsilon\right) \\ &= a\left(\sum_{T\in\mathcal{T}_H} \sum_{i\in\mathring{\mathcal{D}}_H\cap T} \alpha_i\lambda_i^T,\ \epsilon\right)_T - a\left(\sum_{T\in\mathcal{T}_H} \sum_{i\in\mathring{\mathcal{D}}_H\cap T} \alpha_i q_i^T,\ \epsilon\right)\end{aligned}$$

$$
\begin{aligned}
&= \sum_{T\in\mathcal{T}_H}\sum_{i\in\mathring{\mathcal{D}}_H\cap T}\alpha_i\Big[a\left(\lambda_i^T,\epsilon\right)_T - a\left(q_i^T,\epsilon\right)\Big]\\
&= \sum_{T\in\mathcal{T}_H}\sum_{i\in\mathring{\mathcal{D}}_H\cap T}\alpha_i\Big[a\left(\lambda_i^T,\epsilon-w^T\right)_T - a\left(q_i^T,\epsilon-w^T\right)\Big]\\
&= \sum_{T\in\mathcal{T}_H}\left[a\left(\sum_{i\in\mathring{\mathcal{D}}_H\cap T}\alpha_i\lambda_i^T,\epsilon-w^T\right)_T - a\left(\sum_{i\in\mathring{\mathcal{D}}_H\cap T}\alpha_i q_i^T,\epsilon-w^T\right)\right]\\
&= \sum_{T\in\mathcal{T}_H} a\left(u_{\mathrm{LOD}}^T,\epsilon-w^T\right), \qquad (5.10)
\end{aligned}
$$

where $u_{\mathrm{LOD}}^T = \sum_{i\in\mathring{\mathcal{D}}_H\cap T}\alpha_i(\lambda_i^T - q_i^T)$. We are interested in cell residuals on the form $|||u_{\mathrm{LOD}}^T|||_{U_k(T)\setminus U_{k-m}(T)}$, $m<k$, because such residuals, unlike $|||u_{\mathrm{LOD}}^T||| = |||u_{\mathrm{LOD}}^T|||_{U_k(T)}$, are expected to decay exponentially with the patch size k. This is the reason why we utilized the local corrector problem (3.9) in (5.10); we can seek a w^T such that $w^T=\epsilon$ on $U_{k-m}(T)$, with m to be determined.

According to Lemma 5.1 there exists some $v\in\underset{\sim}{V}_h$ such that

$$
\begin{aligned}
I_H v &= I_H\mathcal{I}_h(\eta_{k-1}^T\epsilon),\\
\mathrm{supp}(v) &\subset \mathrm{supp}\left(I_H\mathcal{I}_h(\eta_{k-1}^T\epsilon)\right),
\end{aligned}
$$

where $\eta_{k-1}^T\epsilon$ is the component wise multiplication of η_{k-1}^T and ϵ, and where $\mathcal{I}_h$ is the linear interpolation operator introduced in Section 2.2, which is required because $\eta_{k-1}^T\epsilon$ does not necessarily lie in $\underset{\sim}{V}_h$. We know that $\mathcal{I}_h(\eta_{k-1}^T\epsilon)=\mathcal{I}_h(\epsilon)=\epsilon\in\underset{\sim}{W}_h$ on $\Omega\setminus U_{k-1}(T)$ and $\mathcal{I}_h(\eta_{k-1}^T\epsilon)=(0,0)^{\mathrm{t}}\in\underset{\sim}{W}_h$ on $U_{k-2}(T)$. Now recall the definition of the Clément operator in (3.1). Given a coarse node j, the nodal value $\left(I_H\mathcal{I}_h(\eta_{k-1}^T\epsilon)\right)(j)$ is zero if $\mathcal{I}_h(\eta_{k-1}^T\epsilon)\in\underset{\sim}{W}_h$ on $\mathrm{supp}(\lambda_j)$. Therefore, we can estimate the support of v by extending the ring $U_{k-1}(T)\setminus U_{k-2}(T)$ with one layer on each side,

$$
\mathrm{supp}(v)\subset\mathrm{supp}\left(I_H\mathcal{I}_h(\eta_{k-1}^T\epsilon)\right)\subset U_k(T)\setminus U_{k-3}(T).
$$

Define $\tilde{w}=\mathcal{I}_h(\eta_{k-1}^T\epsilon)-v\in\mathring{\underset{\sim}{W}}_h\left(\Omega\setminus U_{k-3}(T)\right)$. Then $w^T=\epsilon-\tilde{w}$ has the desired properties since $w^T\in\mathring{\underset{\sim}{W}}_h\left(U_k(T)\right)$ and $w^T=\epsilon$ on $U_{k-3}(T)$.

Continuing from (5.10),

$$
\begin{aligned}
\mathrm{II} &= \sum_{T\in\mathcal{T}_H} a\left(u_{\mathrm{LOD}}^T,\epsilon-w^T\right) = \sum_{T\in\mathcal{T}_H} a\left(u_{\mathrm{LOD}}^T,\epsilon-w^T\right)_{U_k(T)\setminus U_{k-3}(T)}\\
&\le \sum_{T\in\mathcal{T}_H}|||u_{\mathrm{LOD}}^T|||_{U_k(T)\setminus U_{k-3}(T)}|||e-w^T|||_{U_k(T)\setminus U_{k-3}(T)}\\
&\overset{\mathrm{CS}}{\lesssim} K^{1/2}|||\epsilon-w^T|||\left[\sum_{T\in\mathcal{T}_H}|||u_{\mathrm{LOD}}^T|||^2_{U_k(T)\setminus U_{k-3}(T)}\right]^{1/2}, \qquad (5.12)
\end{aligned}
$$

where $K^{1/2}$ enters because at most $C_r K$ patches overlap a single element when the norms are taken over the rings $U_k(T) \setminus U_{k-3}(T)$.

The factor $|||\epsilon - w^T||| = |||\tilde{w}|||$ can be bounded in terms of $|||\epsilon|||$ since

$$|||\epsilon - w^T||| \lesssim |||\eta_{k-1}^T \epsilon||| + |||\eta_{k-1}^T \epsilon - \tilde{w}|||,$$

where

$$\begin{aligned} |||\eta_{k-1}^T \epsilon||| &\lesssim \left\| \operatorname{diag}\left(\eta_{k-1}^T\right) \nabla \epsilon \right\| + \left\| \operatorname{diag}(\epsilon) \nabla \eta_{k-1}^T \right\| \\ &\leq \|\nabla \epsilon\| + \frac{1}{H^2} \|\epsilon\|_{U_{k-1}(T) \setminus U_{k-2}(T)} \\ &\overset{(3.2)}{\lesssim} |||\epsilon||| + \frac{1}{H^2} \cdot H^2 |||\epsilon|||_{U_k(T) \setminus U_{k-3}(T)} \\ &\lesssim |||\epsilon|||, \end{aligned}$$

and

$$|||\eta_{k-1}^T \epsilon - \tilde{w}||| \lesssim |||\epsilon|||$$

by Lemma A.2 in [8]. Here $\operatorname{diag}(v)$ denotes the diagonal matrix $\left(\begin{smallmatrix} v_1 & 0 \\ 0 & v_2 \end{smallmatrix}\right)$. We get

$$|||\epsilon - w^T||| \lesssim |||\epsilon||| \overset{(5.8)}{\lesssim} K |||e_h|||. \tag{5.13}$$

Finally, we insert (5.13) into (5.12), which together with (5.9) yield

$$|||e_h|||^2 \lesssim K |||e_h||| \left[\sum_{T \in \mathcal{T}_H} H_T^2 \|f\|_T^2 \right]^{1/2} + K^{3/2} |||e_h||| \left[\sum_{T \in \mathcal{T}_H} |||u_{\mathrm{LOD}}^T|||_{U_k(T) \setminus U_{k-3}(T)}^2 \right]^{1/2}.$$

This proves the theorem. □

5.1 Basic adaptive algorithm for error reduction

The first term in the error estimate (5.2) is dependent on the coarse mesh $\mathcal{T}_H$ due to the element diamaters H_T. The second term captures errors resulting from the restrictions of corrector problems to patches. This means that if the residual $H_T^2 \|f\|_T^2$ is large the coarse mesh needs to be refined on T, and if the residual $|||u_{\mathrm{LOD}}^T|||_{U_k(T) \setminus U_{k-3}(T)}^2$ is large the patch size around T needs to be increased.

The usability of the estimate (5.2) is not high in practice because the second term requires that we use large patch sizes. To be exact, each element patch needs to have at least three layers. Previous results [8] tell us that sometimes only two layers are enough to reduce most of the error due to localization. Having good (in the sense of removing most of the error) initial parameter values essentially defeats the purpose an adaptive

algorithm, which is to change the values only if it is necessary to do so. However, we can, inspired by (5.2), propose an adaptive algorithm that uses only the outermost ring of the patch to compute residuals, which allows us to start with a small patch size. Defining indicators

$$I_1 = c_1 K \sqrt{\sum_{T\in\mathcal{T}_H} H_T^2 \|f\|_T^2} \qquad \text{and} \qquad I_2 = c_2 K^{3/2} \sqrt{\sum_{T\in\mathcal{T}_H} |||u_{\mathrm{LOD}}^T|||^2_{U_k(T)\setminus U_{k-1}(T)}}, \tag{5.14}$$

we attempt to estimate the error $|||u_h - u_{\mathrm{LOD}}|||$ by $I_1 + I_2$. Observe the difference between I_2 and the second term in (5.2). The algorithm requires a calibration phase in which the two constants c_1 and c_2, previously hidden in the symbol $\lesssim$, are estimated. The calibration uses the reference solution u_h and consists of two runs.

1. Set each patch size k to a large number, making I_2 small. Compute $|||u_h - u_{\mathrm{LOD}}^T|||$ and I_1 for decreasing H. The scaling constant c_1 can be estimated by comparing the two convergence plots.
2. Set $H > h$ to a small number, making I_1 small. Compute $|||u_h - u_{\mathrm{LOD}}^T|||$ and I_2 for increasing k. The scaling constant c_2 can be estimated by comparing the two convergence plots.

We can now formulate the algorithm, see Algorithm 5.1 on the next page. This algorithm is rudimentary because H and k are changed globally, i.e. $H_T = H$ and $k(T) = K$ for all $T \in \mathcal{T}_H$ in every iteration. This is a big drawback because if only certain areas of the domain need special attention, refinement should take place only in those areas; the very purpose of a posteriori error algorithms is to avoid computations if they are unnecessary, i.e. if residuals are small. It is easy to implement local patch increase based on residuals rather than on I_2, but to combine it with local refinement of $\mathcal{T}_H$ based on residuals rather than on I_1 would require some work. All that being said, it is of interest to use the proposed algorithm in problems with fine scale features throughout the domain and see how the largest error contributor changes before the tolerance is reached. While we do need u_h in the calibration phase in order to estimate c_1 and c_2, the same constants could hopefully be reused later in other problems with similar material data.

Algorithm 5.1: Adaptive error reduction based on H and k

Data: given are problem data, h, $\mathcal{T}_h$, c_1, c_2, and a reasonable *tolerance*
Result: sufficiently small estimation of *error*

begin
  set initial values H and k, create $\mathcal{T}_H$, assume $error > tolerance$
  while $error > tolerance$ **do**
    compute u_{LOD}^T
    for $T \in \mathcal{T}_H$ **do**
      $R_1(T) = H^2 \|f\|_T^2$
      $R_2(T) = |||u_{\mathrm{LOD}}^T|||^2_{U_k(T)\setminus U_{k-1}(T)}$
    end
    $I_1 = c_1 k \sqrt{\sum_{T\in\mathcal{T}_H} R_1(T)}$
    $I_2 = c_2 k^{3/2} \sqrt{\sum_{T\in\mathcal{T}_H} R_2(T)}$
    $error = I_1 + I_2$
    if $I_1 \geq I_2$ & $2^{-4}H > h$ **then**
      decrease coarse mesh size: $H \longleftarrow H \cdot 2^{-1}$
      refine $\mathcal{T}_H$
    else
      increase patch size: $k \longleftarrow k + 1$
    end
  end
end

6

Numerical experiments

We test the proposed LOD method on two problems and investigate some of its properties. The first problem is an academic problem, meaning that the Lamé parameters and other data are chosen so that the solution is appropriate, i.e. so that the obtained displacements are reasonably large (recall that we assume small displacements). We also use the material from this problem to try out the adaptive algorithm presented in Section 5.1. The second problem is directly related to common techniques that are practiced to analyze heterogeneous materials.

In what follows, an obtained approximation is compared with the reference solution $u_h \in \underset{\sim}{V}_h$. (Recall from Section 2.2 that $\underset{\sim}{V}_h$ captures the fine scale features and therefore u_h is sufficiently close to the exact solution in the sense of Theorem 2.3.) We sometimes use relative (and slightly more representative) errors

$$|||u_h - v|||^{\text{rel}} = \frac{|||u_h - v|||}{|||u_h|||}.$$

All problems are formulated on the unit square $\Omega = (0,1) \times (0,1)$. Both $\mathcal{T}_H$ and $\mathcal{T}_h$ are uniform, and two examples of triangulations can be seen in Figure 4.1, where the mesh sizes are 2^{-2} and 2^{-5}. We refrain from using units since this allows for a tidier presentation of the problems and the results. Solutions are plotted component wise, where the first and second components give the horizontal and vertical displacements, respectively.

6.1 Problem 1: study of a grainy material reinforced with a grid

In this section we take a look at the convergence of our LOD method and compare it to that of the standard method. Conclusion 3.9 in [8] suggests that linear convergence in the energy norm should be achieved for our LOD method by increasing the patch size

k as $\log(H^{-1})$. Therefore, we choose k with this in mind. Note, however, that since we use element patches from Definition 3.1, k still has to be an integer.

We consider the elasticity problem (2.3) with $f = (0.5, 0.5)^{\mathrm{t}}$,

$$\begin{aligned} u &= (0,0)^{\mathrm{t}} && \text{on } \Gamma_D, \\ \sigma(u)\, n &= \left(-0.1 \cdot (\mathrm{e}^{xy} - 1), -0.1 \cdot (\mathrm{e}^{xy} - 1)\right)^{\mathrm{t}} && \text{on } \Gamma_N, \end{aligned}$$

and Lamé parameters as detailed in Figure 6.1. The left and bottom edges of the domain make up Γ_D, and the right and top edges make up Γ_N. The traction $\sigma(u)\, n$ tries to counteract the body load f. It is strongest in the corner $(1,1)^{\mathrm{t}}$ and decreases along both directions of Γ_N. The resolution of the material is such that one pixel corresponds to two elements (a square) in the fine mesh. The resolution of the image in Figure 6.1 is 128x128 pixels, so that $h = 2^{-7}$.

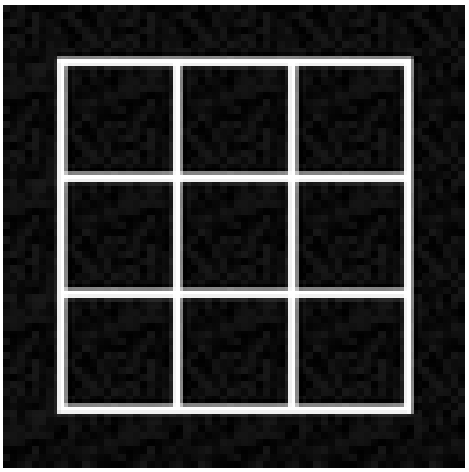

Figure 6.1. Model material in Problem 1. The colors correspond to different values of λ and μ. The matrix is a grainy material where the Lamé parameters are piecewise constant and vary randomly in the interval $0.100 \leq \mu = \lambda \leq 3.085$. The white part of the figure represents a reinforcing grid with $\mu = \lambda = 20$.

Standard FE approximations u_H and LOD approximations u_{LOD} are obtained for several coarse meshes, see Table 6.1. The table shows how the relative errors decrease with H and that the errors are much larger for the standard FEM. The errors are also plotted in Figure 6.2 in order to give a clearer view of the rate of convergence in H. The fitting tells us that $|||u_h - u_{\mathrm{LOD}}|||^{\mathrm{rel}}$ converges approximately linearly with H. Hence, the linear convergence in H, predicted in [8] for their method, can be seen here as well. Meanwhile, the convergence rate is far from optimal for the standard FEM.

Figure 6.3 shows surface plots of u_h, u_{LOD}, and u_H for $H = 2^{-4}$ and $k = 3$. The same functions are plotted in two dimensions in Figure 6.4, with the actual deformation of

the domain included. These figures show that the standard FEM is unable to accurately approximate the solution, which is expected since the coarse mesh is unable to capture all the variations in the material. This illustrates the issue (see end of Section 2.2) with the standard FEM for these kinds of problems. The LOD approximation is good and almost no difference between u_{LOD} and u_h can be spotted. It resolves both the grid and the grainy matrix (look e.g. at the Neumann boundaries in Figure 6.3).

Table 6.1. Relative errors for different coarse mesh sizes H and patch sizes k, where k has been chosen such that it increases approximately as $\log(H^{-1})$. The computations are made for $h = 2^{-7}$.

H	k	$\|\|\|u_h - u_{\text{LOD}}\|\|\|^{\text{rel}}$	$\|\|\|u_h - u_H\|\|\|^{\text{rel}}$
2^{-2}	1	0.11270	8.56897
2^{-3}	2	0.05551	1.32241
2^{-4}	3	0.01892	1.01872
2^{-5}	3	0.01404	0.85341
2^{-6}	4	0.00689	0.48779

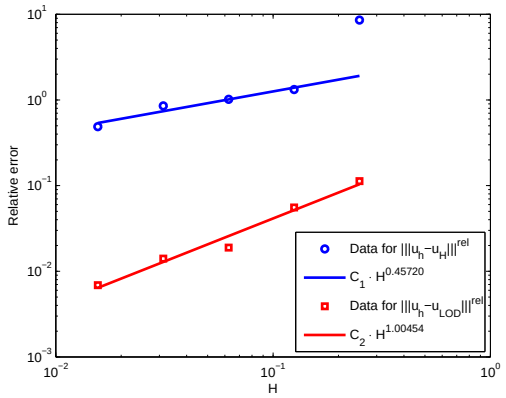

Figure 6.2. The third and fourth column from Table 6.1 drawn in a log-log diagram together with corresponding fits. The circular value at $H = 2^{-2}$ is considered an outlier (2^{-2} is a big mesh size and it is not surprising that the standard FEM becomes completely inadequate at this point) and is therefore not accounted for in the fitting. The fits give indications of the order of convergence and show that it is approximately linear in H for $|||u_h - u_{\text{LOD}}|||^{\text{rel}}$, but far from optimal for $|||u_h - u_H|||^{\text{rel}}$.

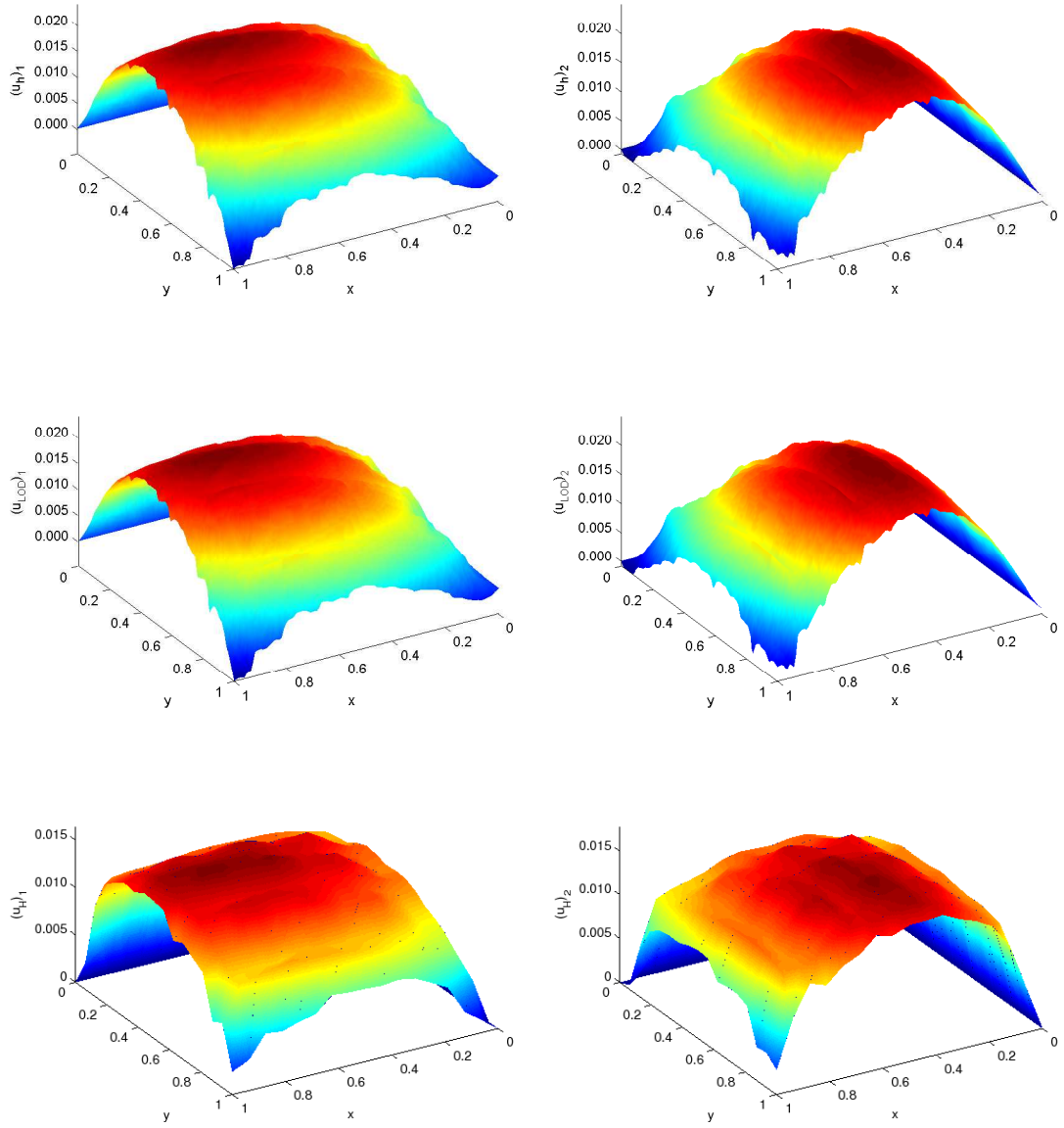

Figure 6.3. A selection of computed solutions represented as surface plots. These ones are obtained for $h = 2^{-7}$ and $H = 2^{-4}$. The top pair shows u_h, the middle pair shows u_{LOD} for $k = 3$, and the bottom pair shows u_H.

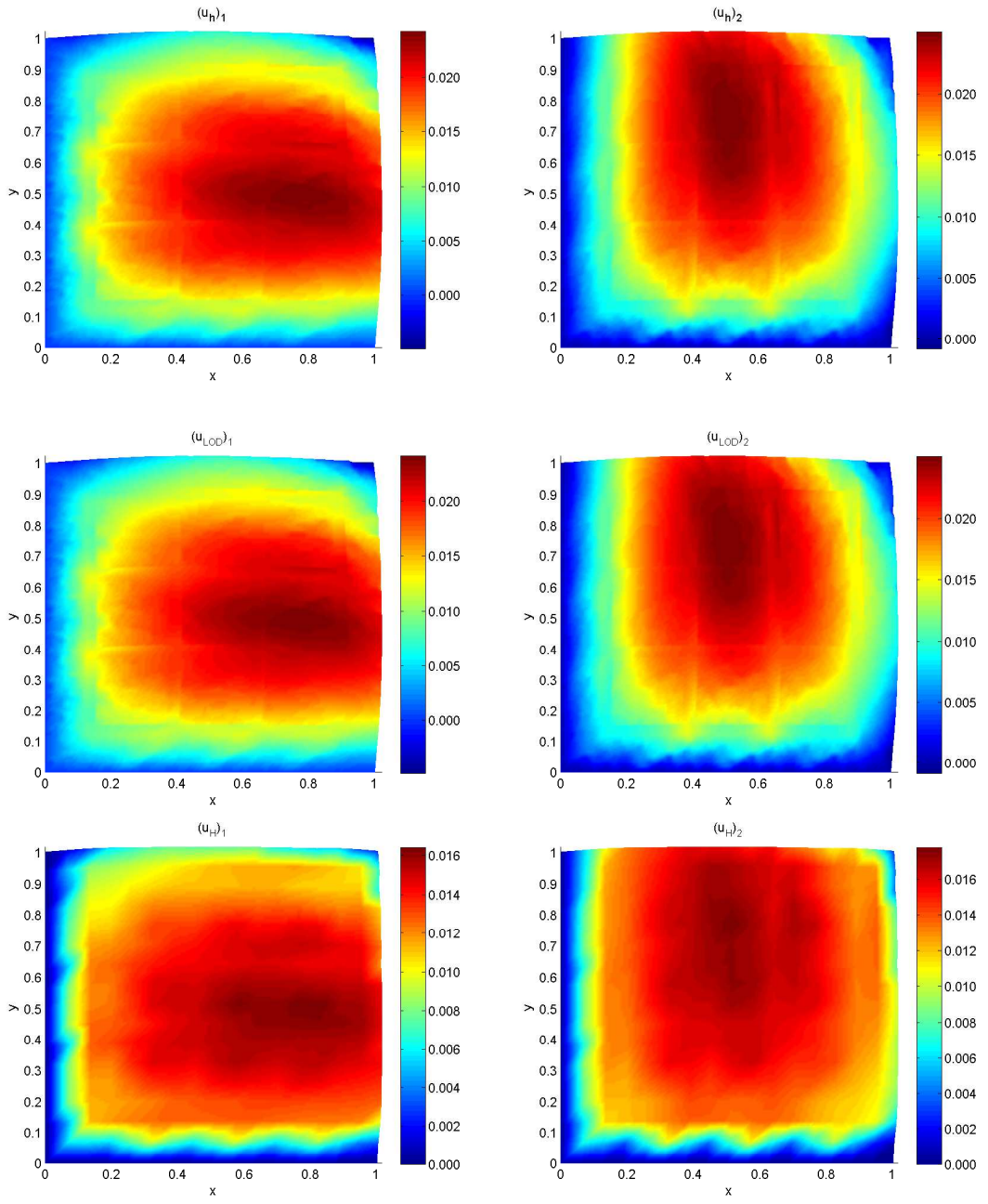

Figure 6.4. A selection of computed solutions represented as two-dimensional plots on the deformed domain. These ones are obtained for $h = 2^{-7}$ and $H = 2^{-4}$. The top pair shows u_h, the middle pair shows u_{LOD} for $k = 3$, and the bottom pair shows u_H.

6.1.1 Adaptive algorithm

We use the material in Figure 6.1 to try out the algorithm presented in Section 5.1. We consider the elasticity problem (2.3) with $f = (0.5, 0.5)^{\mathrm{t}}$ and a homogeneous Dirichlet boundary; $u = (0, 0)^{\mathrm{t}}$ on $\Gamma_D = \partial\Omega$.

The calibration constants c_1 and c_2 are obtained from two separate runs. In the first run we want the residuals R_2 (and hence I_2) to be small and we thus choose a large patch size $k = 5$. The problem is solved four times for decreasing H. Both $|||u_h - u_{\mathrm{LOD}}|||$ and I_1 are computed in each step, see Figure 6.5(a). We fit the data and obtain coefficients. The perfect linear convergence in H of I_1 is expected since f is constant on Ω. In the second run we want I_1 to be small and therefore we choose a small $H = 2^{-5}$. We get the data shown in Figure 6.5(b) by varying k. Now, the simplest way to estimate a calibration constant is to choose values such that the coefficients in the two fits become equal. In other words, we try to align the fit of the indicator with the reference fit. With this approach we find $c_1 = 0.11159/5.0000 = 0.02232$ and $c_2 = 0.00775/0.12989 = 0.05967$.

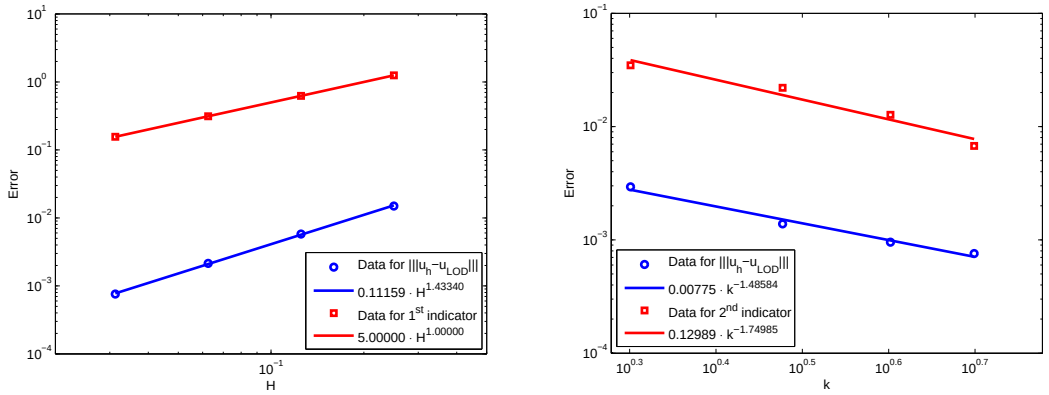

(a) **(b)**

Figure 6.5. Data used in the calibration step shown in log-log diagrams. In (a) we let $k = 5$ and vary H. The two fits allow us to estimate c_1 as $0.11159/5.0000 = 0.02232$. In (b) we let $H = 2^{-5}$ and vary k. The two fits allow us to estimate c_2 as $0.00775/0.12989 = 0.05967$.

The choice of fit when estimating c_2 is not entirely clear. For instance, an exponential fit rather then a power law fit is better for the second indicator data due to the exponential decay of the correctors in u_{LOD}^T. Ideally, judging from (5.14), we would like to use a fit on the form $\alpha k^\beta \gamma^k$.[1] However, we need to choose a function that can fit both data sets well, not only the data for the second indicator. The error due to H is still present in the data for $|||u_h - u_{\mathrm{LOD}}|||$ and the suggested function does not fit this data well. For the current problem, an exponential fit gives $c_2 = 0.05709$, which is close to the first value

[1] In Section 3.2 we used an expected exponential decay of the correctors to justify the localization of corrector problems. We also had this decay in mind during the proof of Theorem 5.2. The data for the second indicator is perfectly fitted by a funtion on the form $\alpha k^\beta \gamma^k$, which indicates that our correctors indeed have the same decay property as the correctors in [8].

that we use in what follows. We realize that estimations can be improved by continued data analysis, but the obtained constants are good enough for our purpose.

We are now ready to use Algorithm 5.1. The initial parameter values are set to $H = 2^{-2}$ and $k = 1$, and the tolerance is set to 0.005. The result is collected in Figure 6.6 and Table 6.2. Six iterations are required in order to reach the tolerance level. In each iteration the algorithm decides which parameter to change based on the sizes of I_1 and I_2. These decisions are included in the figure. We also include $|||u_h - u_{\text{LOD}}|||$ for comparison.

Apart from the first data point, the a posteriori error manages to estimate the real error fairly well. 96% of the error after the first iteration is due to I_2. This suggests that the modified residual, proposed in Section 5.1, is not very good at estimating the error due to localization when $k = 1$. However, this is not true for $k \geq 2$.

Table 6.2 tells us that the error does in actuality reach the tolerance level during the fourth iteration. It is possible that a more careful choice of calibration constants could have saved us two iterations, especially in this problem since $I_1 + I_2$ comes close to the threshold during the fourth iteration. If this is the case, we do at the same time realize that decent results can be obtained even if c_1 and c_2 are not calibrated perfectly. This motivates the possibility to reuse calibration constants for problems with similar data. Realistically, our tolerance is perhaps unnecessarily low, but it lets us test and demonstrate the algorithm, which is the main goal here.

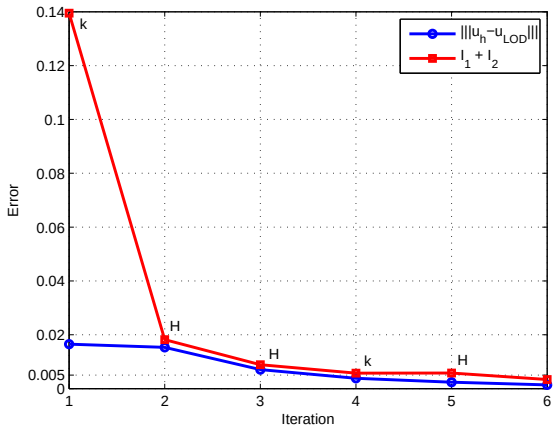

Iter.	$I_1 + I_2$	$\|\|\|u_h - u_{\text{LOD}}\|\|\|$
1	0.13947	0.01650
2	0.01820	0.01533
3	0.00886	0.00705
4	0.00573	0.00383
5	0.00579	0.00239
6	0.00340	0.00138

Figure 6.6 & Table 6.2. Errors computed by the adaptive algorithm. The actual errors are included for comparison. Computations are made for h^{-7} and initial values $H = 2^{-2}$, $k = 1$. The parameter responsible for the largest error in each iteration is indicated. The tolerance level 0.005 is reached when $H = 2^{-5}$ and $k = 3$.

6.2 Problem 2: study of a representative volume element

In this section we look at a type of problem that is widely used in applications where composite materials need to be analyzed. The problem is a part of so called homogenization techniques that makes it possible to obtain information about the macroscopic

properties of a material while only looking at a small part of it. We include this kind of problem in the thesis because it is interesting to give an example of direct applications of the LOD method.

Consider a heterogeneous material with complete scale separation. In this section we solve the elasticity problem on a representative volume element (RVE). An RVE is a part of the material in which all the microstructures in the material can be distinguished. It therefore contains information about the heterogeneties and acts as a representation of the material. Let σ and ε be the stress and strain fields in our RVE. The heterogeneous structure on the subscale influences the macroscopic behavior of the material; it amounts to effective properties of the material on the macroscale. These properties are given by the effective stiffness tensor $\bar{E}$ (recall Hooke's law from Chapter 2). Good approximations of $\bar{E}$ can be obtained from computations on the RVE with certain boundary conditions. The choice of boundary conditions should be such that the so called Hill condition is satisfied (there are three different types of boundary conditions that make sure that this happens, but we only look at one here), see for example [15]. The above only acts as a motivation and we do not go deeper into the theory; our only goal here is to solve the problem on the RVE, and we do not continue further and try to compute $\bar{E}$. It suffices to know that the following boundary condition is not chosen arbitrarily.

Specifically, we consider the elasticity problem (2.3) with Lamé parameters as detailed in Figure 6.7, $f = (0,0)^{\mathrm{t}}$, $\partial\Omega = \Gamma_D$, and $u = \bar{\varepsilon}\,(x,y)^{\mathrm{t}}$ on Γ_D, where the effective

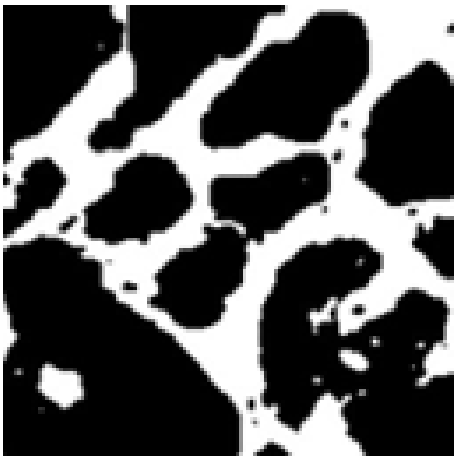

Figure 6.7. RVE used in Problem 2. Its size is about $(110\,\mu\mathrm{m})^2$ and the material is an Al-Cu (black and white, respectively) alloy. The actual contrasts $\mu_{\mathrm{Cu}}/\mu_{\mathrm{Al}}$ and $\lambda_{\mathrm{Cu}}/\lambda_{\mathrm{Al}}$ are fairly low, and because we assign a displacement on the boundary, the small variations are dominated by the displacements enforced by the boundary condition. Therefore, we increase the contrast and set $\mu_{\mathrm{Al}} = \lambda_{\mathrm{Al}} = 1$, $\mu_{\mathrm{Cu}} = 50$, and $\lambda_{\mathrm{Cu}} = 100$ to easier spot the variations in the solution.

strain $\bar{\varepsilon}$ is constant and prescribed a priori. Examples of three interesting cases are

$$\bar{\varepsilon} = \begin{pmatrix} a & 0 \\ 0 & 0 \end{pmatrix}, \quad \bar{\varepsilon} = \begin{pmatrix} 0 & 0 \\ 0 & a \end{pmatrix} \quad \text{and} \quad \bar{\varepsilon} = \begin{pmatrix} 0 & a \\ a & 0 \end{pmatrix}$$

for $a \ll |\Omega|^{1/2}$, which correspond to a horizontal normal strain, a vertical normal strain and a pure shear strain, respectively. We use the third matrix in our problem and set $a = 0.05$. Some results from the computations are shown in Figure 6.8. The bottom part shows u_{LOD} when $H = 2^{-4}$ and $k = 2$. The relative error is $|||u_h - u_{\text{LOD}}|||^{\text{rel}} = 0.01565$. We see from the figure that u_{LOD} is a fairly good approximation even though we use only 2 patch layers. The applied boundary condition is the dominating contributor to the shape of the solution, but there are a few interfaces that are clearly discernable. There are some irregularities in the approximation compared to u_h, e.g. in the bottom right corner, which is the most demanding area as can be seen in 6.7.

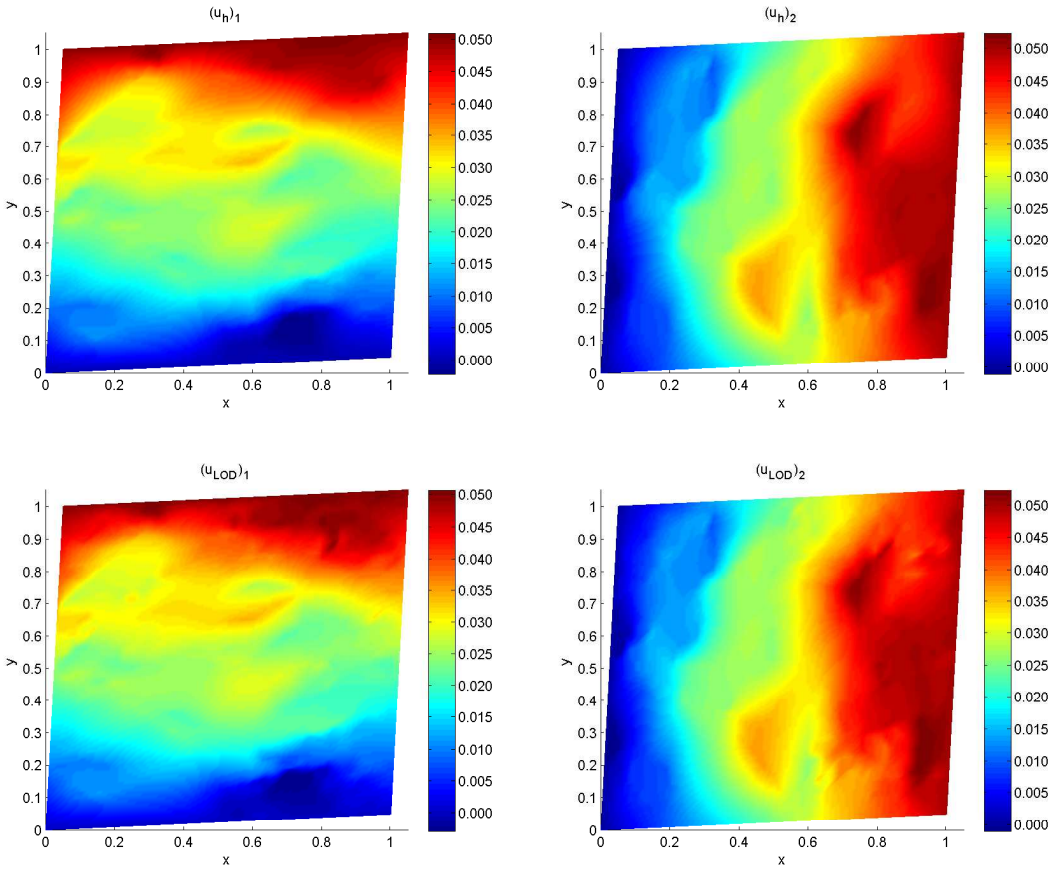

Figure 6.8. A selection of computed solutions represented as two-dimensional plots on the deformed domain. The computations are made for $h = 2^{-7}$. The top pair shows u_h and the bottom pair shows u_{LOD} for $H = 2^{-4}$ and $k = 2$.

7

Conclusion

We have introduced the LOD method to problems in linear elasticity. In the previous chapter the method was successfully used to solve (2.3) with strongly heterogeneous data. Convergence of the method was verified. In particular, the common linear convergence in H was obtained by choosing patch sizes k properly. The expected exponential decay of the correctors was observed.

An a posteriori error estimate was proven in Theorem 5.2. Here the next step is to extend it so that not only homogeneous Dirichlet problems can be analyzed a posteriori, but any mixed boundary problem. Inspired by the estimate, we proposed an adaptive algorithm for error reduction. The algorithm managed to make pretty good estimations of the errors and adapt to them. At this point, however, the algorithm is rudimentary because it does not allow for a non-uniform refinement of the coarse mesh. Ideally we want a method that can control all parameters: the fine mesh size, coarse mesh size, and patch size. The computational effort is heavily dependent on h. For an adaptive algorithm to have any further practical use it also has to take the fine mesh size h into account.

Hopefully the method will be applied to more problems in solid mechanics in the future. In fact, the method is not particularly efficient when it comes to solving stationary PDEs like the ones in this thesis. This is because the multiscale basis that is computed is used only one time, i.e. only one multiscale problem is solved. While the multiscale system (4.9) is a lot cheaper than the standard problem (4.2), the rather large computational cost of computing the basis makes it not worth to use the LOD method. Therefore, these problems could be solved more efficiently with other methods, like the multigrid method. The LOD method is better suited for non-linear (see e.g. [9]) or time-dependent (see e.g. [12]) problems that are solved iteratively, because the basis can be reused in each iteration. The method is also advantageous for problems with a huge amount of DOFs that makes them nearly impossible to solve with the standard FEM even once. That being said, it has still been useful to apply the method on a relatively simple problem as an initial step. Our LOD solver could be developed further

and be used to solve the elastic wave propagation problem, for example. It is similar to the elasticity problem (2.3), except that (2.3a) is replaced with a wave equation $\rho\frac{\partial^2 u}{\partial t^2} - \nabla \cdot \sigma(u) = f$, where ρ is the density of the medium, and initial conditions are required. The next appropriate step could be to study this problem.

References

[1] R. E. Bank and H. Yserentant, *On the H^1-stability of the L^2-projection onto finite element spaces*. Numer. Math. 126 (2014), pp. 361-381.

[2] S. Brenner and L. R. Scott, *The Mathematical Theory of Finite Element Methods*. 3rd edition. Springer-Verlag, 2008.

[3] S. Brenner and L.-Y Sung, *Linear finite element methods for planar linear elasticity*. Mathematics of Computation 59 (1992), pp. 321-338.

[4] C. Carstensen and R. Verfürth, *Edge residuals dominate a posteriori error estimates for low order finite element methods*. SIAM J. Numer. Anal. 36 (1999), pp. 1571-1587.

[5] J.-M. Drezet, B. Mireux, Z. Szaraz and T. Pirling, *In situ Neutron Diffraction during Casting: Determination of Rigidity Point in Grain Refined Al-Cu Alloys*. Materials 7 (2014), pp. 1165-1172

[6] G. Duvaut and J.L. Lions, *Inequalities in Mechanics and Physics*. Springer-Verlag, 1976.

[7] Y. Efendiev and T. Hou, *Multiscale Finite Element Methods: Theory and Applications*. Springer-Verlag, 2009.

[8] P. Henning and A. Målqvist, *Localized orthogonal decomposition techniques for boundary value problems*. SIAM J. Sci. Comp. 36 (2014), pp. A1609-A1634.

[9] P. Henning, A. Målqvist and D.Peterseim, *A localized orthogonal decomposition method for semi-linear elliptic problems*. ESAIM: Mathematical Modelling and Numerical Analysis 48 (2014), pp. 1331-1349.

[10] T.J.R. Hughes, G.R. Feijoo, L. Mazzei and J.-B. Quincy, *The variational multiscale method – a paradigm for computational mechanics*. Comp. Meth. Appl. Mech. Eng. 166 (1998), pp. 3-24.

[11] M. Larson and F. Bengzon, *The Finite Element Method: Theory, Implementation and Applications*. Springer-Verlag, 2013.

[12] A. Målqvist and A. Persson, *Multiscale techniques for parabolic equations*. Submitted, available from `http://arxiv.org/abs/1212.0090`.

[13] A. Målqvist and D. Peterseim, *Computation of eigenvalues by numerical upscaling*. Numer. Math. 130 (2015), pp. 337-361.

[14] A. Målqvist and D.Peterseim, *Localization of elliptic multiscale problems*. Math. Comp. 83 (2014), pp. 2583-2603.

[15] M. Ostoja-Starzewski, *Material spatial randomness: From statistical to representative volume element*. Probab. Eng. Mech. 21 (2006), pp. 112–132.